

國立交通大學  
光電工程研究所

碩士論文

量子點面射型雷射動態特性之研究

**Dynamical Characteristics of Quantum Dot Vertical  
Cavity Surface Emitting Laser**

研究生：葉晁恩

指導教授：郭浩中 教授

盧廷昌 教授

中華民國九十七年七月

量子點面射型雷射動態特性之研究

**Dynamical Characteristics of Quantum Dot Vertical  
Cavity Surface Emitting Laser**

研究生: 葉晁恩	Student: Chao-En Yeh
指導教授: 郭浩中 教授	Advisor: Prof. Hao-Chung Kuo
盧廷昌 教授	Prof. Tien-Chang Lu

國立交通大學  
光電工程研究所  
碩士論文

A Thesis  
Submitted to Institute of Electro-Optical Engineering  
College of Electrical Engineering  
National Chiao Tung University  
in Partial Fulfillment of the Requirements  
for the Degree of  
Master  
In  
Electro-Optical Engineering

July 2007  
Hsinchu, Taiwan, Republic of China

# 量子點面射型雷射之動態特性研究

研究生：葉晁恩

指導教授：郭浩中教授  
盧廷昌教授

國立交通大學光電工程研究所

## 摘要

本論文主旨在研究量子點面射型雷射的動態特性分析。論文分為兩大部分，第一部分為  $0.98\mu\text{m}$  量子點面射型雷射的量測，首先介紹元件的結構與 L-I-V 曲線。並展示了，在不同溫度下元件的頻率響應、相對雜訊。然後利用校正的方法求出元件本質的頻率響應，並且分析比較實驗的量測數據。這部份的最近是做元件非線性失真的觀察和展示在不同溫度下 2.5Gb/s 的眼圖。第二部分為  $1.3\mu\text{m}$  量子點面射型雷射的量測，一開始是介紹元件的結構與 L-I-V 曲線。接下來展示分別在有與無外部注入光源的情況下做，相對雜訊的量測，我們觀察到在有外部注入光的情況下，雷射共振頻率可以大幅提升，同時我們也對量測相對雜訊的結果做模擬分析。第一部分的最後是對有量子點與量子井結構的面射型雷射之 Linewidth enhancement factor 做比較與討論。這些成果將有助於面射型雷射在光通訊的發展。

# Dynamical Characteristics of Quantum Dot Vertical Cavity Surface Emitting Laser

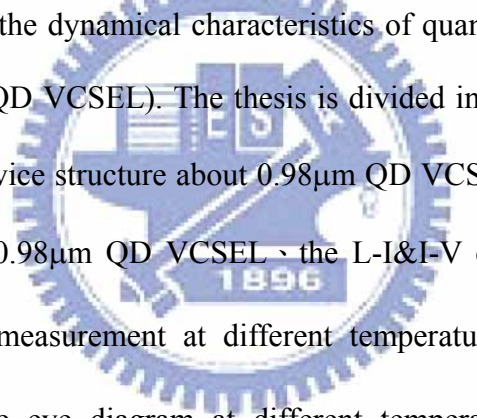
Student : Chao-En Yeh

Advisor : Prof. Hao-Chung Kuo  
Prof. Tien-Chang Lu

National Chiao Tung University

Department of Photonics & Institute of Electro-Optical Engineering

## Abstract



In this thesis, we study the dynamical characteristics of quantum dots vertical cavity surface-emitting laser (QD VCSEL). The thesis is divided into two parts. In the first parts, we present the device structure about  $0.98\mu\text{m}$  QD VCSEL. We also present the device structure about  $0.98\mu\text{m}$  QD VCSEL, the L-I&I-V curves, the relative intensity noise (RIN) measurement at different temperature, frequency response calibration method, the eye diagram at different temperature and the nonlinear distortion. We also use the calibration method to find the device frequency response. In the second part of this thesis, we report the dynamic characteristics of the  $1.3\mu\text{m}$  QD VCSEL, the L-I&I-V curves, RIN measurement of the device with light injection and without light injection, the simulation results of RIN spectrum and linewidth enhancement factor. Comparing with QD and QW structure, we can observe active layers with QD structure having small linewidth enhancement factor at different bias current.

## Acknowledgment

(誌謝)

本論文能夠順利完成，首先要感謝我的指導老師郭浩中教授的督促、王興宗老師和盧廷昌教授的糾正、彭朋群教授的指導，使得我學習到做研究嚴謹的態度和邏輯的思考以及表達能力的訓練與方法等等。感謝老師們的教誨，兩年的碩士生涯要過去了，進入半導體雷射實驗室讓我成長了許多，這些過程對我將會是十分寶貴的經驗。



在這兩年的碩士生活中，彭朋群老師像是學長一樣照顧我，在實驗的過程中給我方向與指導，在 401 的日子中憲哥和俊榮學長們都很照顧我們這些學弟，帶給我們很珍貴的回憶，伯駿、柏源、卓木和尚樺都是一起吃飯的好夥伴，帶給我碩士生活中不一樣的記憶。還有在實驗室共同奮鬥的同學們和博士班學長和學弟妹們，使我能順利的完成碩士班的考驗。

最後，謹將本論文獻給我的家人。謝謝他們兩年來的支持與鼓勵，使我能順利完成學位。

# Contents

Abstract (in Chinese).....	i
Abstract (in English).....	ii
Acknowledgement.....	iii
Contents.....	iv
Chapter 1 Introduction	
1-1 Introduction of Quantum Dot VCSEL.....	1
1-2 Review of Injection locking technique.....	1
1-3 Review of Linewidth enhancement factor.....	2
1-4 Organization of the Dissertation.....	4
Chapter 2 Dynamical characteristics of 0.98 $\mu\text{m}$ QD VCSEL	
2-1 Sample structure and Fabrication process.....	7
2-2 DC Characteristics of QD VCSEL.....	7
2-3 Frequency Response.....	8
2-4 RIN measurement.....	12
2-5 Frequency Response Calibration.....	13
2-6 Eye diagram.....	14
2-7 Nonlinear characteristic measurement.....	16
2-8 Summary.....	18
Chapter 3 Dynamical characteristics of 1.3 $\mu\text{m}$ QD VCSEL	
3-1 Sample structure and Fabrication process.....	28
3-2 DC Characteristics of QD VCSEL.....	29
3-3 RIN measurement.....	30
3-4 Simulations.....	34
3-5 Linewidth enhancement factor.....	37
3-6 Summary.....	42

## Chapter 4 Summary

4-1 Summary.....	51
4-2 Future Work.....	52
Fig 2-1 the structure of the 0.98 $\mu$ m VCSEL with SML QD.....	20
Fig 2-2 I-V and L-I curve of the 0.98 $\mu$ m QD VCSEL at different temperature.....	20
Fig 2-3 experimental setup for measurement frequency response.....	21
Fig 2-4 frequency response of the device at different temperature.....	21
Fig 2-5 RIN spectrum at different current and temperature.....	22
Fig 2-6 compare calibration result resonant frequency with RIN peak.....	23
Fig 2-7 experimental setup for measurement eye diagram.....	24
Fig 2-8 the eye diagram of the device with 2.5 Gb/s.....	24
Fig 2-9 the parameter obtain from eye diagram.....	25
Fig 2-10 experimental setup for measurement nonlinear distortion.....	25
Fig 2-11 the nonlinear distortion at 2mA BW=3Hz.....	26
Fig 2-12 (a) the second harmonic distortion (b) the third harmonic distortion at 2mA and resolution is 3kz.....	26
Fig 2-13 the nonlinear distortion at different RF power ( BW : 30kHz ).....	27
Fig 2-14 the nonlinear distortion at different modulation frequency (BW:30kHz).....	27
Fig 3-1 the structure of 1.3 $\mu$ m QD VCSEL.....	44
Fig 3-2 experimental setup for measurement DC characteristic.....	44
Fig 3-3 I-V and L-I curve of the 1.3 $\mu$ m QD VCSEL (No. 15) .....	45
Fig 3-4 Optical spectrum of the device at different current .....	45
Fig 3-5 experiment setup for the RIN measurement .....	46
Fig 3-6 RIN spectrum of the device without external light injection.....	46

Fig 3-7 RIN spectrum for the device with external light injection.....47

Fig 3-8 the optical spectrum of the device with and without light injection.....47

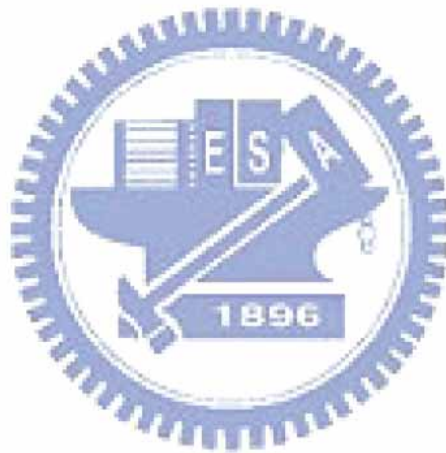
Fig 3-9 stimulation result of the RIN spectrum with external light injection.....48

Fig 3-10 stimulation result of the frequency response with external light injection.....48

Fig 3-11 Compare the RIN peaks with the resonant frequency with external light injection.....49

Fig 3-12 experiment setup for the locking region measurement.....49

Fig 3-13 linewidth enhancement factor of the device with QD and QW structure at different current.....50





## **Chapter 1 Introduction**

### **1-1 Introduction of Quantum Dot VCSEL**

Vertical-cavity surface-emitting lasers (VCSELs) have been researched in recent year. The reduction of the gain length has to compensate by a high Q cavity. There are some advantages of VCSELs, such as low power consumption, circular beam and 2D integrator resulting in important applications in optical fiber communications. Recently, QD structure with some ultra advantages in active layer has been studied [1-3]. The density of state of the QD structure is discrete energy levels, because it is atom-like. Active layer with QD structure has some advantages, such as ultra low threshold current [4-5], higher deferential gain, lower linewidth enhancement factor and insensitive in different temperature. VCSELs at around  $1.3\mu\text{m}$  fabricated on GaAs substrates have been expected to realize high-performance and low-cost light sources for fiber communication systems. The large conduction offset improves the temperature performance over that of conventional InP-based materials.

### **1-2 Review of Injection locking technique**

Injection locking technique has been studied for many years. In 1980 Kobayashi and Kimura used GaAs lasers to demonstrate the injection locking experimental results. [6] Using two devices with close wavelength is necessary. In 2005 Lukas Chrostowski, Xiaoxue Zhao and Connie J Chang-Hasnain used  $1.55\mu\text{m}$  VCSEL to

demonstrate the resonance frequency enhanced from 7GHz up to ~50GHz [7]. The technique is that one laser the master laser (ML) is external light source to inject photons in another laser the slave laser (SL). The physical reason of the resonant frequency enhancement might result from the external light inject into the slave laser as a cavity increase the photons in the slave laser. Using the technique has some advantages, such as side-mode suppression, enhancement the relaxation oscillation, improvement nonlinear characteristic and chip, reducing noise. It makes direct modulation more suites for many applications.

For CATV and fiber radio systems, the direct modulation of semiconductor lasers can be used for transmitting subcarrier-multiplexed signals at low cost of using injection locking to improve the nonlinear characteristic.[8] For optical communication, the resonance frequency enhancement by using the injection locking technique means that we will have much larger bandwidth can be used. The technique can greatly improve the operation characteristic give use more freedom to pick device for communication system so that injection-locked direction lasers is a viable way to use for future analog and digital networks.

### **1-3 Review of Linewidth enhancement factor**

In 1981, Fleming and Mooradian demonstrated the linewidth of a semiconductor laser and found the linewidth is different from Schawlow-Townes predicted. They

were unable to explain the result [9]. In 1982, Charles H. Henry wrote a paper about the theory of the linewidth of semiconductor [10]. In general, the phase of the optical field fluctuation to influence the laser linewidth. The fluctuations are due to the spontaneous emission. Linewidth enhancement factor( $\alpha$ ) is the deviation of the imaginary part and real part of the refraction index.

$$\alpha = \frac{\Delta n'}{\Delta n''}$$

The linewidth brooding is attributed to the change in refractive index with carrier density. From the Kramers-Kronig relations, we can find the change in the imaginary part of the susceptibility will change the real part of the susceptibility. A symmetrical gain curve will lead to the dispersion curve of the refractive index has a zero at the frequency corresponding to the gain peak. [11]

Large value of linewidth enhancement factor will result in chirp under direct modulation in optical fiber communication. A symmetric gain spectrum will make linewidth enhancement factor close to zero so that the index of refraction will not change with the carrier density. The quantum dot structure is atom-like. In the theoretically, the density of states of the quantum dot structure is a series of delta-function, its gain spectrum ideally satisfies the criteria.

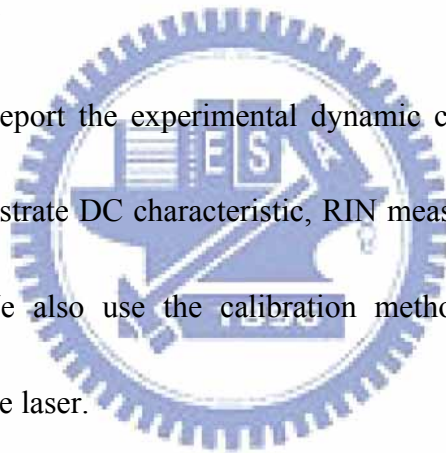
There are sever methods to measure the linewidth enhancement factor, such as RF-modulation measurement, the interferometric measurement, the amplified

spontaneous emission (ASE) method and using the locking region measurement [12]

#### **1-4 Organization of the Dissertation**

This thesis consists of two related parts about two devices respectively. In Chapter 2, we demonstrate 1.3  $\mu\text{m}$  QD VCSELs dynamic properties including DC characteristic, RIN measurement with and without external light injection and linewidth enhancement factor. We also stimulate the RIN spectrum and frequency response. Using the external light injection technique, the device relaxation frequency can be reach to 19.2GHz

In Chapter 3, we report the experimental dynamic characterization of 0.98 $\mu\text{m}$  QD VCSEL. We demonstrate DC characteristic, RIN measurement, eye diagram and nonlinear distortion. We also use the calibration method to obtain the intrinsic frequency response of the laser.



## Reference

- [1] S. L. Chuang, N. Holonyak, Jr. "Quantum-well assisted tunneling injection quantum-dot lasers," *Conference on Lasers and Electro-Optics, Technical Digest*, vol. 1, pp. 297, 2002.
- [2] T. Yang, J. Tatebayashi, S. Tsukamoto and Y. Arakawa," Highly uniform self-assembled InAs/GaAs quantum dots emitting at 1.3 $\mu$ m by metalorganic chemical vapor deposition," *Physica E*, vol. 26, pp. 77-80, 2005.
- [3] N. N. Ledentsov, "Long-wavelength quantum-dot lasers on GaAs substrates: from media to device concepts," *IEEE Journal of Selected Topics in Quantum Electronics*, vol. 8, pp. 1015 - 1024, 2002.
- [4] N. N. Ledentsov, M. Grundmann, F. Heinrichsdor, D. Bimberg, V.M. Ustinov, A. E.Zhukov, M. V. Maximov, Zh. I. Alferov, J. A. Lott, "Quantum-Dot Heterostructure Lasers," *IEEE Journal of Selected Topics in Quantum Electronics*, vol. 6, no. 3, pp. 439-451, 2000.
- [5] J. A. Lott, N. N. Ledentsov, V. M. Ustinov, A. Yu. Egorov, A. E. Zhukov, P. S. Kop'ev, Zh. I. Alferov, and D. Bimberg, "Vertical cavity lasers based on vertically coupled quantum dots," *Electronics Letters*, vol. 33, pp. 1150-1151, 1997.
- [6] S. Kobayashi and T. Kimura,"Coherence on injection phase-locked AlGaAs semiconductor laser," *Electronics Letters*, vol. 16, pp. 668-670, 1980
- [7] Lukas Chrostowski, Xiaoxue Zhao and Connie J. Chang-Hasnain, "50 GHz Directly-Modulated Injection-Locked 1.55  $\mu$ m VCSELs," Optical Society of America, 2005
- [8] Erwin K Lau,"High-Speed Modulation of Optical Injection-Locked Semiconductor Lasers," *Electrical Engineering and Computer Sciences University of California at Berkeley*, 2006
- [9] M. W. Fleming and A. Mooradian, "Fundamental line broadening of single-mode

(GaAl)As diode lasers,” *Appl. Phys. Lett.*, vol. 38, p. 511, 1981.

[10] CHARLES H. HENRY, “Theory of the Linewidth of Semiconductor Lasers,”

*IEEE journal of quantum electronics*, vol. **QE-18**, no. **2**, February **1982**

[11] MAREK OSINSKI and JENS BUUS, “Linewidth Broadening Factor in semiconductor Lasers-An Overview” *Quantum Electronics, IEEE Journal of*, 1987

[12] G. Liu, X. Jin, and S. L. Chuang, “Measurement of Linewidth Enhancement Factor of Semiconductor Lasers Using an Injection-Locking Technique” *IEEE photonics technology letters*, VOL. 13, NO. 5, MAY 2001



## Chapter 2 Dynamical characteristics of 0.98 $\mu\text{m}$ QD VCSEL

### 2-1 Sample structure and Fabrication process

The VCSEL structures were grown on GaAs (001) substrates by molecular-beam epitaxy (MBE) method. The bottom DBR structure consists of 33-pairs n-doped GaAs–Al<sub>0.9</sub>Ga<sub>0.1</sub>As, the cavity is an undoped Al<sub>0.15</sub>Ga<sub>0.85</sub>As and the top DBR consists of 20-pairs p-doped GaAs–Al<sub>0.9</sub>Ga<sub>0.1</sub>As. P-type doping uses Carbon and n-type doping uses silicon [1]. In order to obtain the output wavelength is 0.98 $\mu\text{m}$ , the layer thicknesses and compositions were needed to be designed. To reduce the series resistance, a 10-nm interface region between the GaAs–Al<sub>0.9</sub>Ga<sub>0.1</sub>As DBR layers was modified by linearly composition grading along with relatively high doping. The Al composition profile was achieved by the digital-alloy technique—inserting a monolayer of GaAs after fixed number of monolayer of Al<sub>0.9</sub>Ga<sub>0.1</sub>As. The optical cavity contains the three-stack SML InGaAs QD active region with 8-nm-thick GaAs spacers placed at an antinode of the optical-field intensity. The device structure is shown in Fig.2-1.

### 2-2 DC Characteristics of QD VCSEL

Fig. 2-2 shows the output power of the device versus current curve (L-I). We measure the device L-I at different temperature. We observe the L-I curve are not smooth due to multi transverse mode occur at higher current operate. Fig. 2-2 also

shows the voltage of the device versus current curve (I-V).

## 2-3 Frequency Response

### 2-3-1 Theory

The rate equations describe the carrier number, the photon number and the phase variation. From the rate equation, we can derive the frequency response of the device and the relaxation resonance frequency.

Consider the application a DC current above the threshold current,  $I_0$ , carried with a small AC signal,  $I_m$ , to the device. The small modulation signal with harmonics wave and the frequency is  $\omega$ . Assume  $I_m \ll I_0$  bias and spontaneous emission term,  $\beta$ , is neglected. Small signal can be express as:

$$\begin{aligned} I &= I_0 + I_m(t) = I_0 + I_m(\omega)e^{j\omega t} \\ n &= n_0 + n_m(t) = n_0 + n_m(\omega)e^{j\omega t} \\ n_p &= n_{p0} + n_{pm}(t) = n_{p0} + n_{pm}(\omega)e^{j\omega t} \end{aligned} \quad \text{Eq. 2-3.1}$$

The rate equation can be express as:

$$\begin{aligned} \frac{dn}{dt} &= \frac{I}{qV} - \frac{n}{\tau} - g_0(n - n_{tr})n_p \\ \frac{dn_p}{dt} &= g_0(n - n_{tr})n_p + \beta R_{sp} - \frac{n_p}{\tau_p} \end{aligned} \quad \text{Eq. 2-3.2}$$

Substitute Eq (2-3.1) into Eq(2-3.2), the equation can be rewrite as:



$$\begin{aligned}\frac{dn_m}{dt} &= \frac{I_m}{qV} - \frac{n_m}{\tau} + g_0(n_0)n_{pm} - g_0n_m n_{p0} \\ \frac{dn_{pm}}{dt} &= g_0n_{p0}n_m - g_0(n_0)n_{pm} - \frac{n_{pm}}{\tau_p}\end{aligned}\quad \text{Eq. 2-3.3}$$

Express the rate equations of carrier and photon in frequency domain.

For the carrier equation:

$$\begin{aligned}j\omega n_m(\omega)e^{j\omega t} &= \frac{I_m(\omega)e^{j\omega t}}{qV} - \frac{n_m(\omega)e^{j\omega t}}{\tau} + g_0(n_0)n_{pm}(\omega)e^{j\omega t} - g_0n_{p0}n_m(\omega)e^{j\omega t} \\ \Rightarrow j\omega n_m(\omega) &= \frac{I_m(\omega)}{qV} - \frac{n_m(\omega)}{\tau} + g_0(n_0)n_{pm}(\omega) - g_0n_{p0}n_m(\omega) \\ \Rightarrow [j\omega - g_0n_{p0} + \frac{1}{\tau}]n_m(\omega) &= \frac{I_m(\omega)}{qV} + g_0(n_0)n_{pm}(\omega)\end{aligned}$$

For the photon equation:

$$\begin{aligned}\Rightarrow j\omega n_{pm}(\omega) &= g(n_0)n_{pm}(\omega) + g_0n_{p0}n_m(\omega) - \frac{n_{pm}(\omega)}{\tau_p} \\ \Rightarrow [j\omega - g(n_0) + \frac{1}{\tau_p}]n_{pm}(\omega) &= g_0n_{p0}n_m(\omega)\end{aligned}$$

We obtain two equations relative to the carrier and photon and then solve the two equations to get the carrier and photon equation at frequency domain.

$$\begin{aligned}n_m(\omega) &= \left(\frac{j\omega}{j\omega\Omega - \omega^2 - \omega_r^2}\right)\left(\frac{I_m(\omega)}{qV}\right) \\ n_{pm}(\omega) &= \left(\frac{\tau_p\omega_r^2}{j\omega\Omega - \omega^2 - \omega_r^2}\right)\left(\frac{I_m(\omega)}{qV}\right)\end{aligned}\quad \text{Eq. 2-3.4}$$

$$\omega_r^2 = (2\pi f_r)^2 = \left(\frac{n_{p0}}{\tau_p}\right)g_0; \Omega = \frac{1}{\tau} + n_{p0}g_0$$

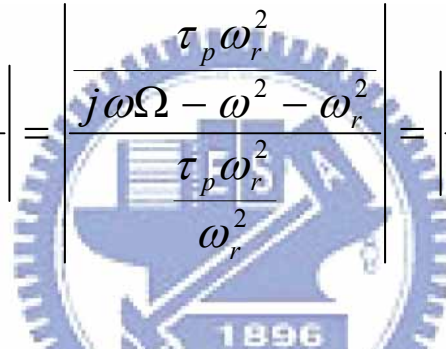
When small signal carrier injection in the diode, it induces photon and oscillation.

This phenomenon can be observed by measuring the frequency response. The natural

frequency of oscillation associated with this mutual dependence between carrier and

photon. Modulation response is expanded the small signal modulation relationship to

steady-state. From Eq. (2-3.4), the modulation response is denoted as

$$H(\omega) = \left| \frac{n_{pm}(\omega)}{n_{pm}(0)} \right| = \left| \frac{\frac{\tau_p \omega_r^2}{j\omega\Omega - \omega^2 - \omega_r^2}}{\frac{\tau_p \omega_r^2}{\omega_r^2}} \right| = \left| \frac{\omega_r^2}{j\omega\Omega - \omega^2 - \omega_r^2} \right|$$


Eq. 2-3.5

Transfer function, H(w), describing the response of the laser intensity at the drive

current with small variations through the active region.

$$H(\omega) = C \frac{f_r^2}{f_r^2 - f^2 + j \frac{f}{2\pi} \gamma}$$

Eq. 2-3.6

$f_r$  : the resonance frequency ;  $\gamma$  : the damping factor ;  $C$  : constant

Taking the carrier transport and parasitic elements into account additional

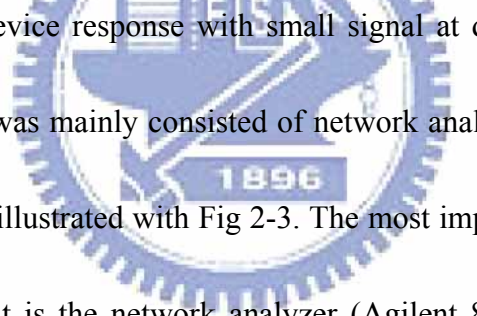
extrinsic limitations related to the laser structure results in an extra pole in the small

signal modulation transfer function.

$$H(\omega) = C \left( \frac{f_r^2}{f_r^2 - f^2 + j \frac{f}{2\pi} \gamma} \right) \cdot \left( \frac{1}{1 + j \frac{f}{f_p}} \right) \quad \text{Eq. 2-3.7}$$

The  $f_p$  is the cutoff frequency due to the parasitic effect, like a low pass filter. For the application in optical communication system, the device can be operated bandwidth is the most important thing. It is crucial for microwave applications that the modulation bandwidth of the VCSEL is sufficiently large so that efficient modulation is achieved as the modulation frequency.

### 2-3-2 Experimental Setup



We measure the device response with small signal at different frequency. The microwave test system was mainly consisted of network analyzer, Bias-Tee and high speed photodetector, as illustrated with Fig 2-3. The most important instrument of the microwave measurement is the network analyzer (Agilent 8720ES). Transmitter of network analyzer produced -10dBm RF signal. Current source (Keithley 238) provided direct bias current with the laser diode. Bias-Tee combined AC and DC signal transmission through the coaxial cable. The laser diode was hermetically sealed by a standard TO-Can laser package (TO-46) with a built-in lens. Then, we welded our device on a high speed SMA connector and connected with the coaxial cable. 25-GHz near-IR photodetector (New Focus, model 1414) was received the modulation light signal from the laser diode and was conversed into electrical signal

and fed to network analyzer. Comparing two channels microwave signal by network analyzer, information of transmission and reflection characteristics could be expressed as vector(magnitude and phase), scalar(magnitude only), phase-only quantities, that was, S-parameter.

### **2-3-3 Frequency Response at different temperature**

The small signal response of VCSELs as a function of bias current was measured at three different temperature using a calibrated vector network analyzer (Agilent 8720ES). We observe the frequency response increasing with current, but the 3dB will be limited about 2 GHz. Bias at higher current, the frequency response will occur notch phenomenon. The notch phenomenon due to multi-mode operates [2]. We can observe the optical spectrum, will show the multi-mode phenomenon. Fig2-4 shows the frequency response at different temperature and different current.

## **2-4 RIN measurement**

### **2-4-1 Experimental Setup**

We measure the relative intensity noise characteristics of the 0.98 $\mu$ m QD VCSEL. We need to setup a system which can test our sample packaged device and can maintain the device temperature. The Scheme of the measurement system includes current source, temperature controller, and RF spectrum analyzer. Keithley

238 is the current source can provide precisely continuous current to laser diode and measure relative voltage synchronously. The temperature controller model is TED200 with station can maintain the environmental temperature. The RIN spectrum is measured by the RF spectrum analyzer (module Hp 8563E). The resolution of RF spectrum analyzer is 30KHz at experiment result.

#### **2-4-2RIN measurement at different temperature**

The RIN peak is a good indicate the relaxation frequency of the device. We experiment at different current and different temperature. We observer the RIN peak can be reach to higher frequency than the resonant frequency of frequency response observed. Because RIN measurement thought as parasitic free, the RIN peak is not equal to resonant frequency observed from frequency response. It due to the package, external circle will limit the performance of the frequency response. The measurement results show in Fig 2-5. The inset chart is the resonant frequency versus current.

### **2-5 Frequency Response Calibration**

#### **2-5-1Theory**

The frequency response we measure involves the frequency response of the device package. Assume the parasitic components of the laser diode are not power dependent. We subtract the laser frequency response of two different current [3]. By

fitting the data, we will get the intrinsic parameter.

The measure data:

$$H_{free}^2(f) = H_{parasitic}^2(f) \cdot \frac{f_{r1}^4}{(f^2 - f_{r1}^2)^2 + \left(\frac{\gamma_{r1}}{2 \cdot \pi}\right)^2 \cdot f^2}$$

Eq. 2-5.1

Subtract the data of two different current:

$$H(f) = 10 \log_{10} \left( \frac{f_{r1}^4}{(f^2 - f_{r1}^2)^2 + \left(\frac{\gamma_{r1}}{2 \cdot \pi}\right)^2 \cdot f^2} \cdot \frac{(f^2 - f_{r2}^2)^2 + \left(\frac{\gamma_{r2}}{2 \cdot \pi}\right)^2 \cdot f^2}{f_{r2}^4} \right)$$

Eq. 2-5.2

We can observe the parasitic term be eliminated.

### 2-5-2 Results and Discussion

We used above method to calibrate the measurement results. By fitting the data got from the substrate two frequency responses at different current at the same temperature, we can get the resonant frequency and compare with the RIN peaks.

Fig 2-6 shows the compare results and the stimulation results.

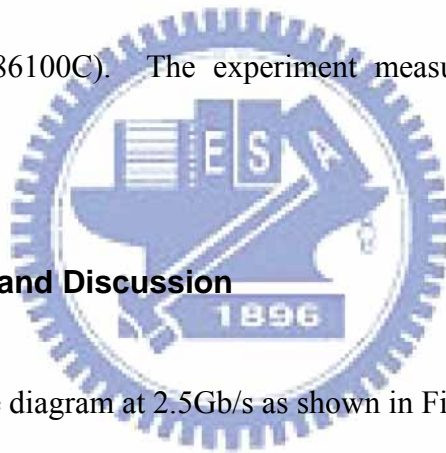
### 2-6 Eye diagram

Eye diagram can measure the optical time domain to characterize system pulse performance in digital optical communication systems. Eye diagram is the multi-value wave from measurement. From the eye diagram, we can obtain the rise time, fall time

and extinction ratio. Eye diagrams are formed by overlaying multiple single-value pseudo-random binary sequence (PRBS) waveforms. The experimental result show on a high speed oscilloscope or eye diagram analyzer.

### **2-6-1 Experimental Setup**

We measure the eye diagram of the 0.98 $\mu$ m QD VCSEL. We need to setup a system which can test our sample. The system includes a trigger signal, Pulse pattern generator (MP1763C), temperature controller, current source and wide-bandwidth oscilloscope (Agilent 86100C). The experiment measurement system shows in Figure 2-7.



### **2-6-2 Results and Discussion**

We illustrate the eye diagram at 2.5Gb/s as shown in Fig 2-8. We observe the eye diagram open and list the parameter got from the eye measurement result. From the extinction ratio value, the 0.98 $\mu$ m QD VCSEL can be used in 2.5Gb/s system. Extinction ratio is the ratio of the maximum value and minimum value. In general, the value should be 6dB. Using the value, we justify the device can be used in system.

## 2-7 Nonlinear characteristic measurement

### 2-7-1 Theory

In optical communication system, we wish the transmission signal is accurate the same as origin signal. However, neither device is perfectly linear, particularly when large modulation levels are involved. Several different types of distortion products are common from these components such as harmonic distortion and inter-modulation distortion. Inter-modulation due to the nonlinear effects may distinct two sources. The first is about the rate equation intrinsic nonlinearities cause by the mixing of photons and electrons in the laser cavity. The second is the nonlinearity of the laser power-current curve [4-5].

The intensity modulated is the laser output power with modulated signal at the modulating frequency. It depends on the linearity of the device and there will also be some modulating power at harmonics of the modulating frequency. It is usually some modulated power at the second harmonic and third harmonic of the modulating frequency. Harmonic distortion is defined as the ratio of modulated power in harmonic of the modulating frequency to the power at the modulating frequency.



$$\begin{aligned}
 HD_2 &= \frac{P(2f_{\text{mod}})}{P(f_{\text{mod}})} \\
 HD_3 &= \frac{P(3f_{\text{mod}})}{P(f_{\text{mod}})} \\
 THD &= \frac{P(2f_{\text{mod}}) + P(3f_{\text{mod}}) + \dots + P(nf_{\text{mod}})}{P(f_{\text{mod}})}
 \end{aligned}$$

Eq. 2-7.1

The  $HD_2$  is the second harmonic distortion,  $HD_3$  is the third harmonic distortion, and THD is the total harmonic distortion

Two closely spaced signals of intermodulation distortion is third-order intermodulation (IMD). This is because the IMD signals fall close to the original modulating frequencies.

$$IMD(2f_i - f_j) = \frac{P(2f_i - f_j)}{P(f_i)}$$

Eq. 2-7.2

### 2-7-2 Experimental Setup

We measure the nonlinear distortion characteristics of the  $0.98\mu\text{m}$  QD VCSEL. We need to setup a system which can test our sample packaged device, signal generator and can maintain the device temperature. The Scheme of the measurement system, illustrates in Figure 2-10, include current source, temperature controller, and RF spectrum analyzer. The signal generator is hp 8657B can generate 0.1~2060 MHz. Keithley 238 is the current source can provide precisely continuous current to laser

diode and measure relative voltage synchronously. The temperature controller model is TED200 with station can maintain the environmental temperature. The nonlinear distortion characteristic is measured by the RF spectrum analyzer (module Hp 8563E). The resolution of RF spectrum analyzer is 1MHz at experiment result.

### **2-7-3 Results and Discussion**

We measure nonlinear characteristic at different RF power at 1GHz and the device bias at 2mA. The experimental result shows in Fig 2-11. From the figure we can obtain SFDR is about 76dB. We also measured the second and third harmonic distortion at different RF power. Finally, we show the nonlinear characteristic at two different conditions. Fig 2-13 shows the device at different RF power. Fig 2-14 shows the device at different modulation frequency.

### **2-8 Summary**

We report the dynamic characteristics of the 0.98 $\mu$ m QD VCSEL. We also present the device structure about 0.98 $\mu$ m QD VCSEL, the L-I&I-V curves, the RIN measurement at different temperature, frequency response calibration method, the eye diagram at different temperature and the nonlinear distortion. The RIN peak is the relaxation frequency. We also use the calibration method to find the device frequency response. A 2.5 Gb/s non-return-to-zero (NRZ) pseudo-random binary sequence (PRBS) data with  $2^{31}-1$  pattern length from a pattern generator used to directly modulate the QD VCSEL. The eye diagrams can be clearly observed. We also measure the nonlinear distortion at different modulation frequency and at different modulation power.

## Reference

- [1] Sergey A. Blokhin, Nikolai A. Maleev, Alexander G. Kuzmenkov, Alexey V. Sakharov, Marina M. Kulagina, Yuri M. Shernyakov, Innokenty I. Novikov, Mikhail V. Maximov, Victor M. Ustinov, Alexey R. Kovsh, Sergey S. Mikhrin, Nikolai N. Ledentsov, Gray Lin, and Jim Y. Chi, "Vertical-Cavity Surface-Emitting Lasers Based on Submonolayer InGaAs Quantum Dots," *IEEE journal of quantum electronics*, VOL. 42, 2006
- [2] Yinon Satuby and Meir Orenstein, "Small-Signal Modulation of Multitransverse Modes Vertical-Cavity Surface-Emitting Semiconductor Lasers," *IEEE photonics technology letters*, VOL. 10, 1998
- [3] P. A. Morton, T. Tanbun-Ek, R. A. Logan, A. M. Sergent, P. F. Sciortino, Jr., and D. L. Coblenz, "Frequency Response Subtraction for Simple Measurement of Intrinsic Laser Dynamic Properties," *Photonics Technology Letters, IEEE*, 1992
- [4] Anders Larsson, Christina Carlsson, Johan Gustavsson, Åsa Haglund, Peter Modh and Jörgen Bengtsson, "Direct high-frequency modulation of VCSELs and applications in fibre optic RF and microwave links," *New J. Phys.* **6**, 2004
- [5] ROBERT OLSHANSKY, VINCENT A. LANZISERA, AND PAUL M. HILL, "Subcarrier Multiplexed Lightwave Systems for Broad-Band Distribution," *journal of lightwave technology*, vol 7, 1989

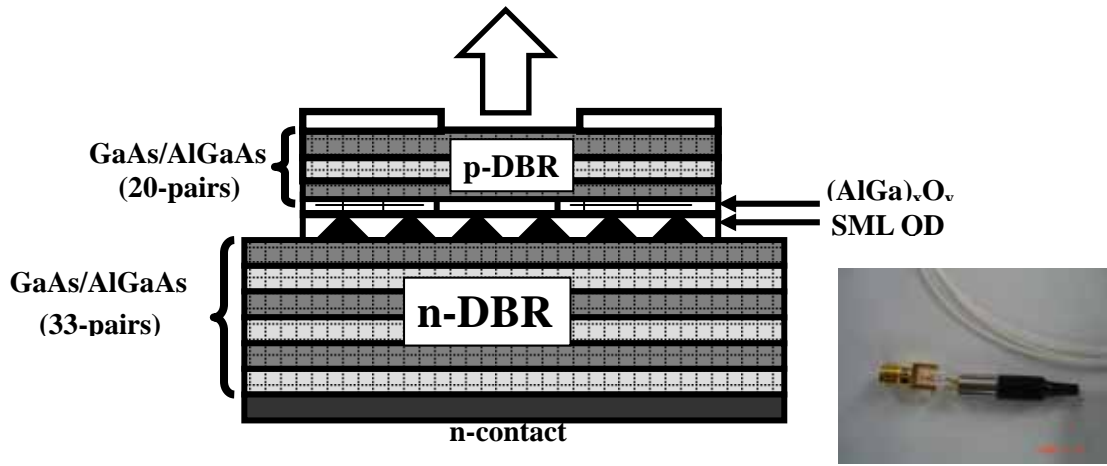


Fig 2-1 The structure of the 0.98  $\mu\text{m}$  VCSEL with SML QD

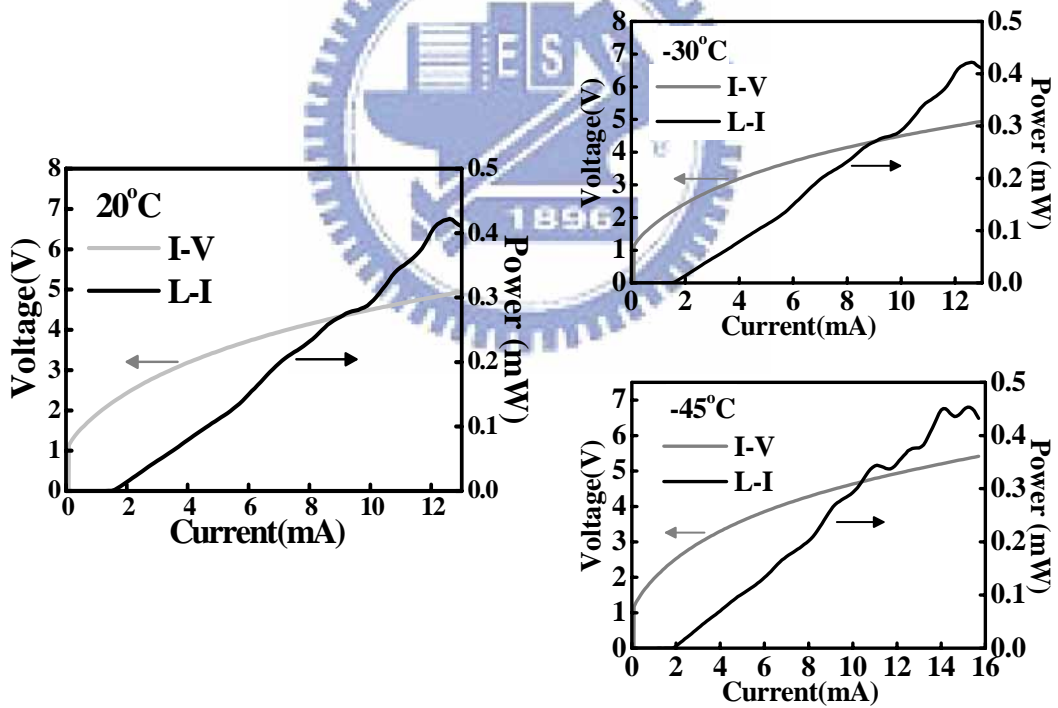


Fig 2-2 I-V and L-I curve of the 0.98 $\mu\text{m}$  QD VCSEL at different temperature

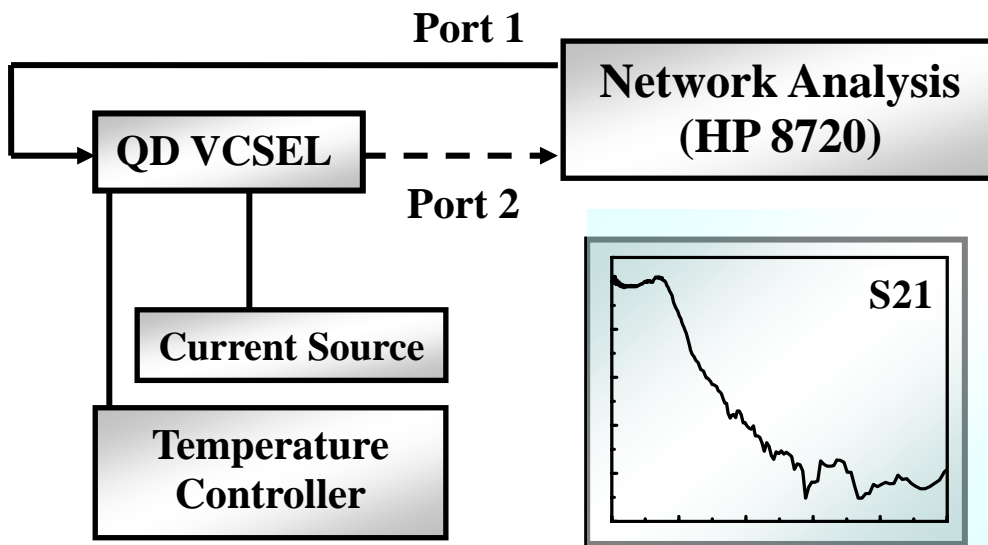


Fig 2-3 experimental setup for measurement frequency response

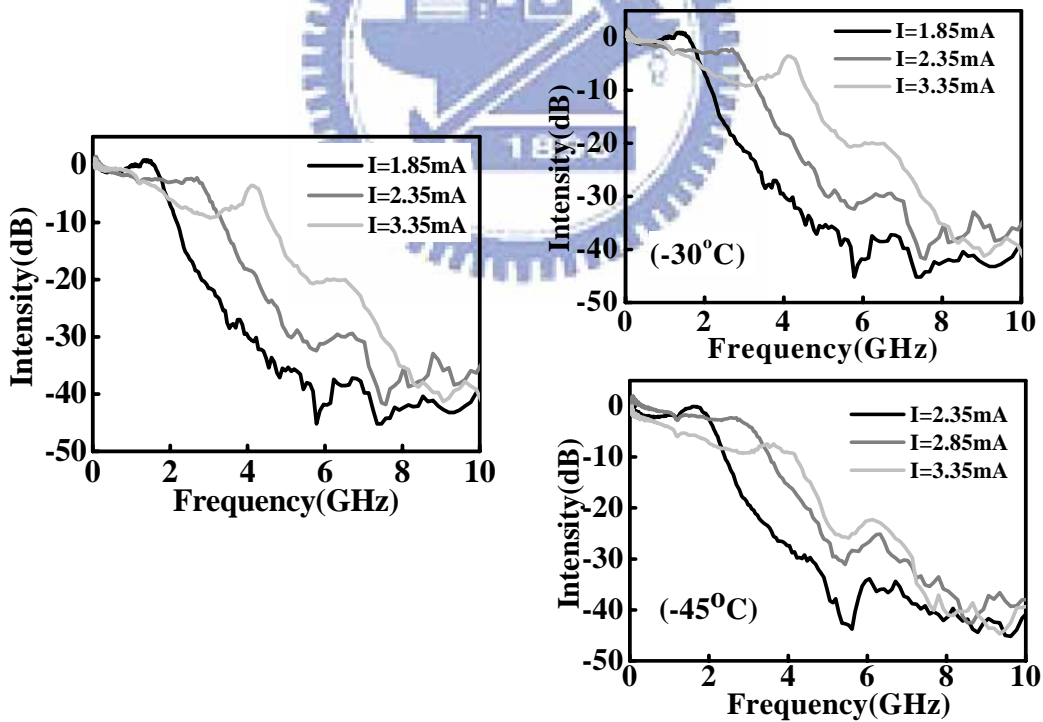


Fig 2-4 frequency response of the device at different temperature

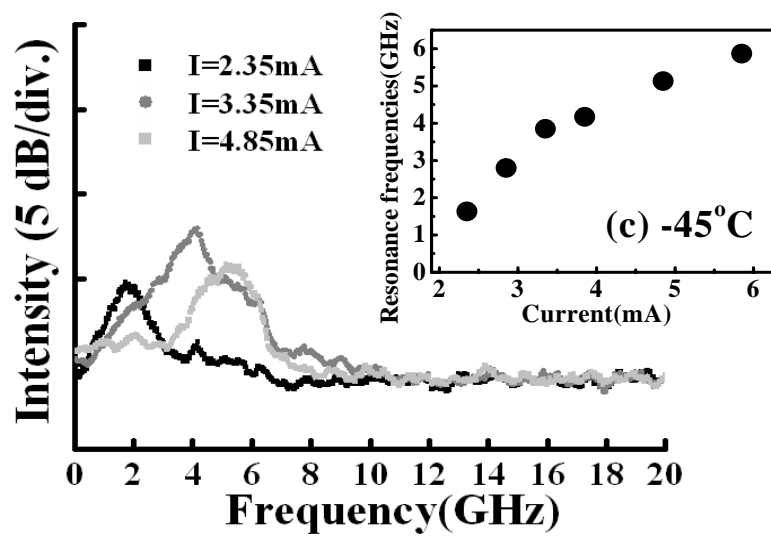
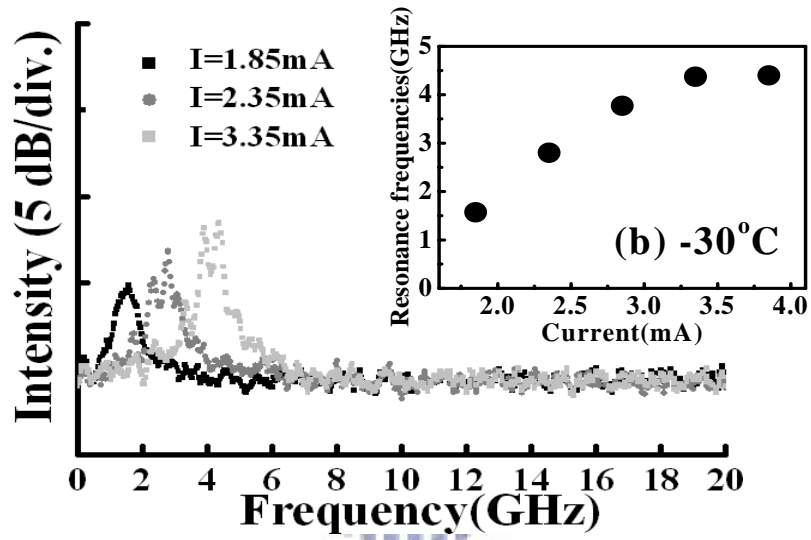
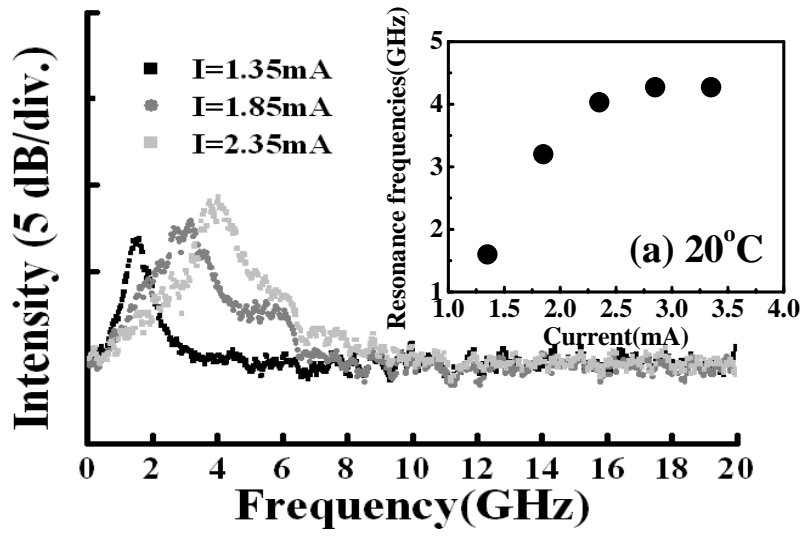


Fig 2-5 RIN spectrum at different current and temperature

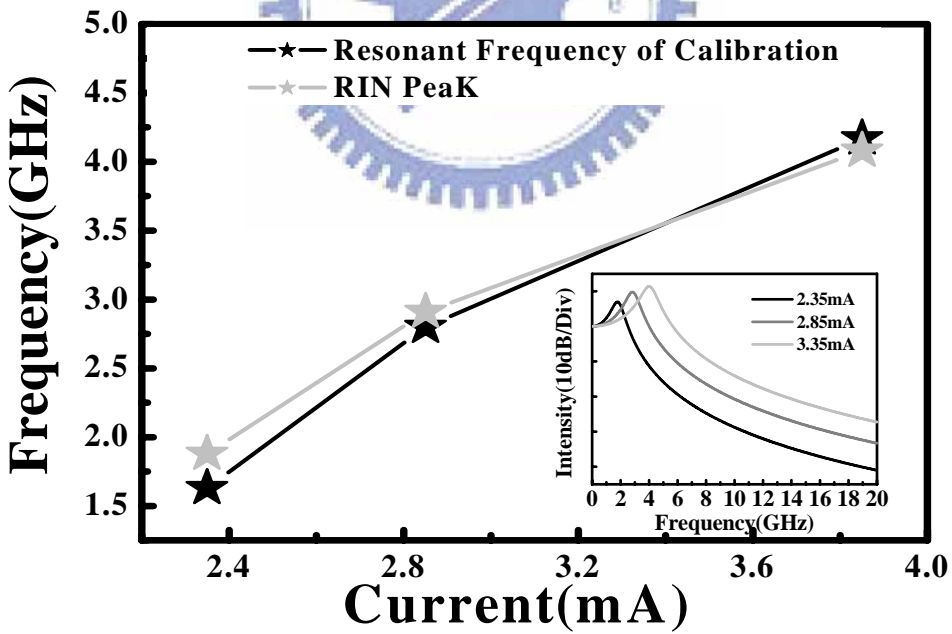
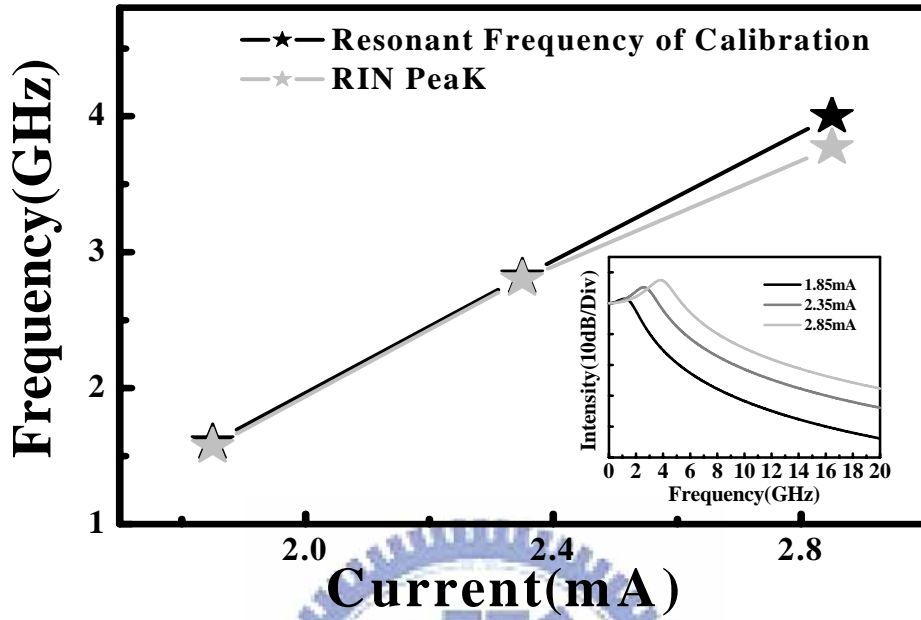


Fig 2-6 compare calibration result resonant frequency with RIN peak

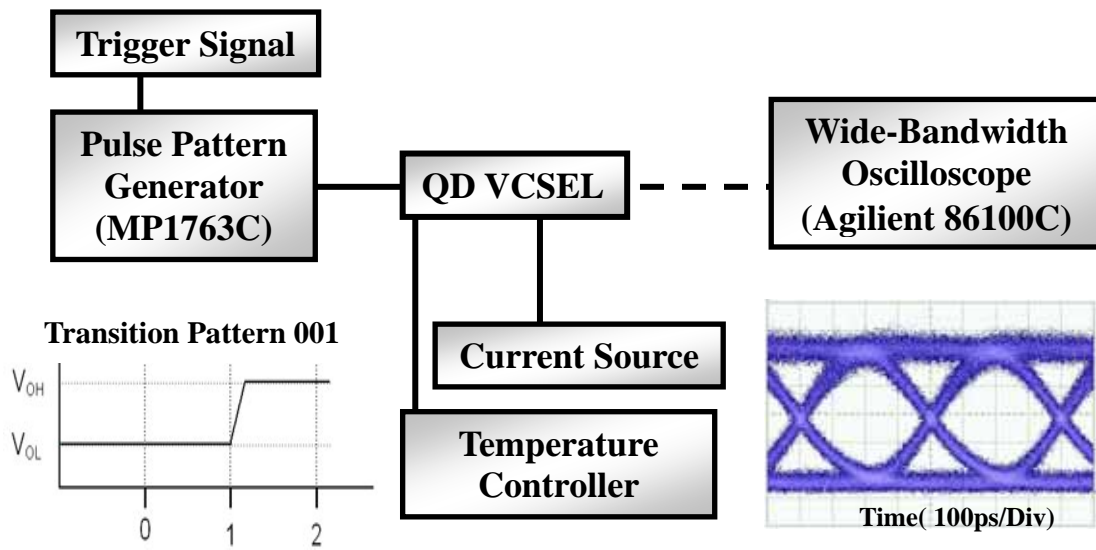


Fig 2-7 experimental setup for measurement eye diagram

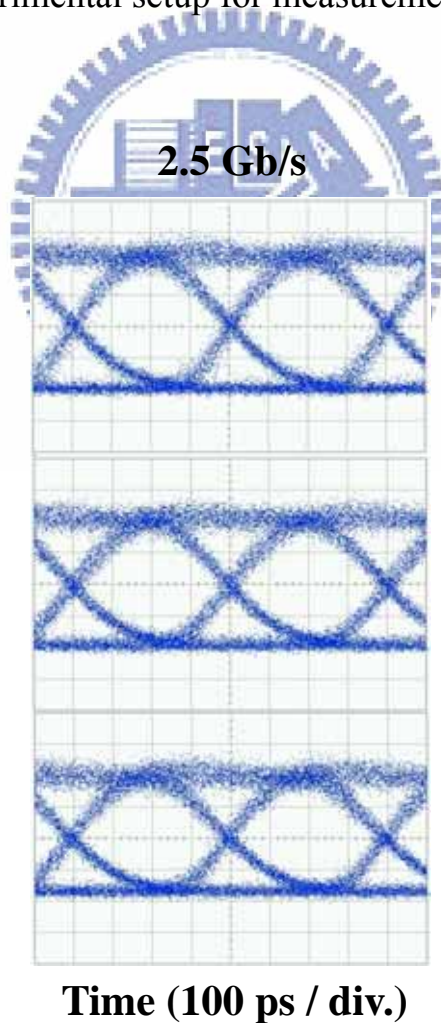


Fig 2-8 the eye diagram of the device with 2.5 Gb/s



Temperature	Extinction Ration	Rise time	Fall time
20°C	12.85dB	82.2ps	222.2ps
-30°C	11.97dB	68.9ps	142.2ps
-45°C	13.07dB	77.8ps	213.3ps

Fig 2-9 the parameter obtain from eye diagram

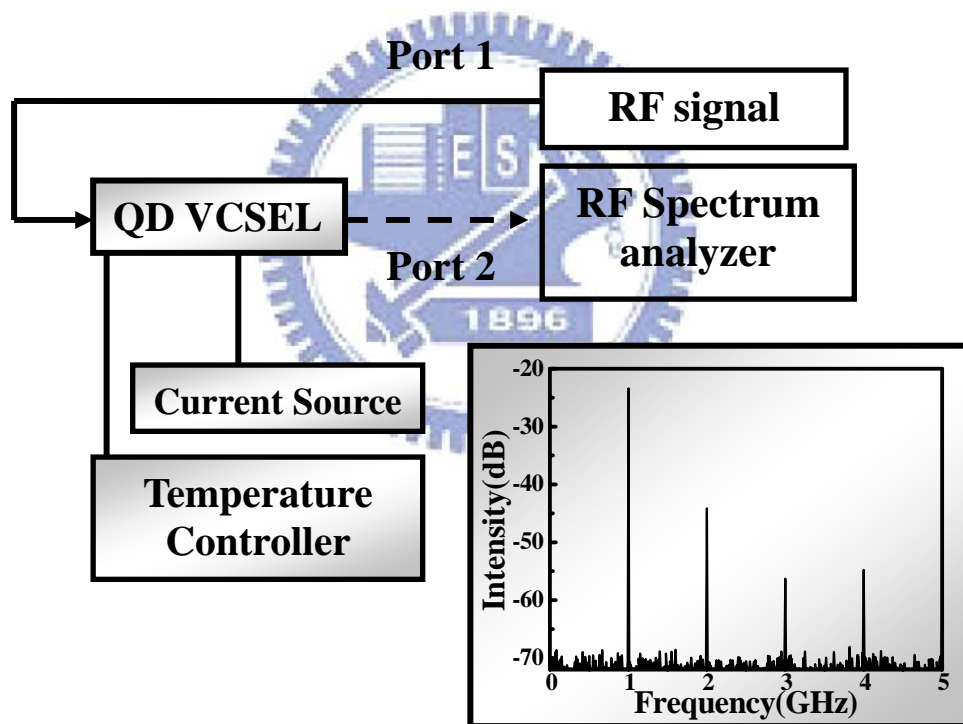


Fig 2-10 experimental setup for measurement nonlinear distortion

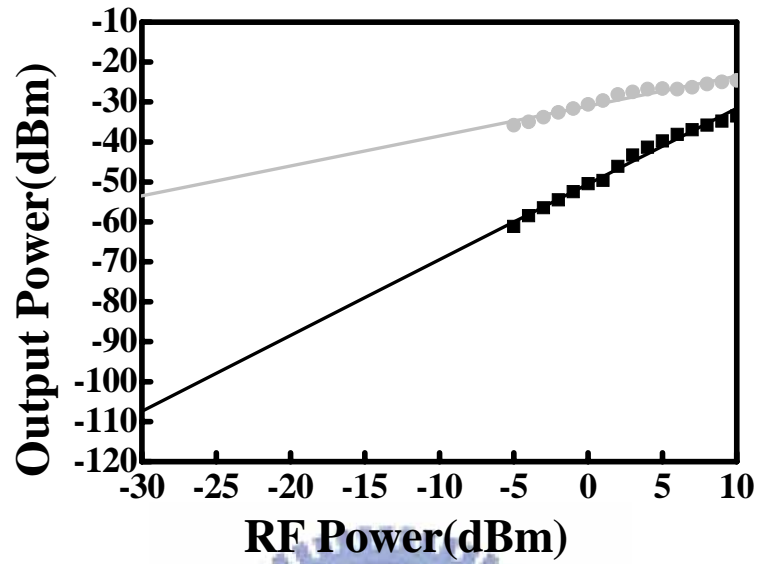


Fig 2-11 the nonlinear distortion at 2mA BW=3Hz

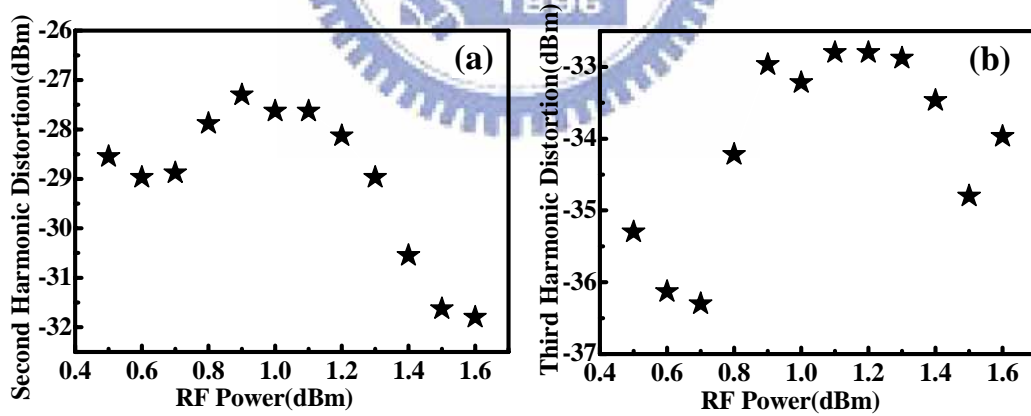


Fig 2-12 (a) the second harmonic distortion (b) the third harmonic distortion at 2mA and resolution is 3kz

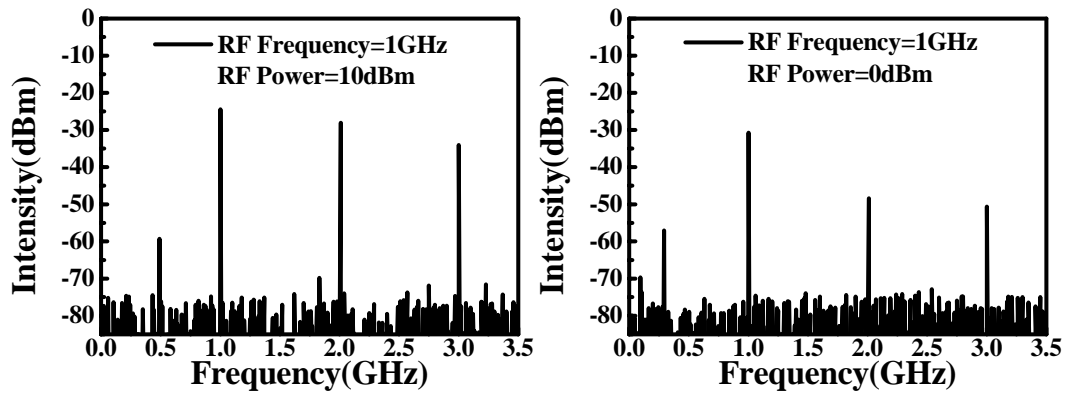


Fig 2-13 the nonlinear distortion at different RF power ( BW : 30kHz )

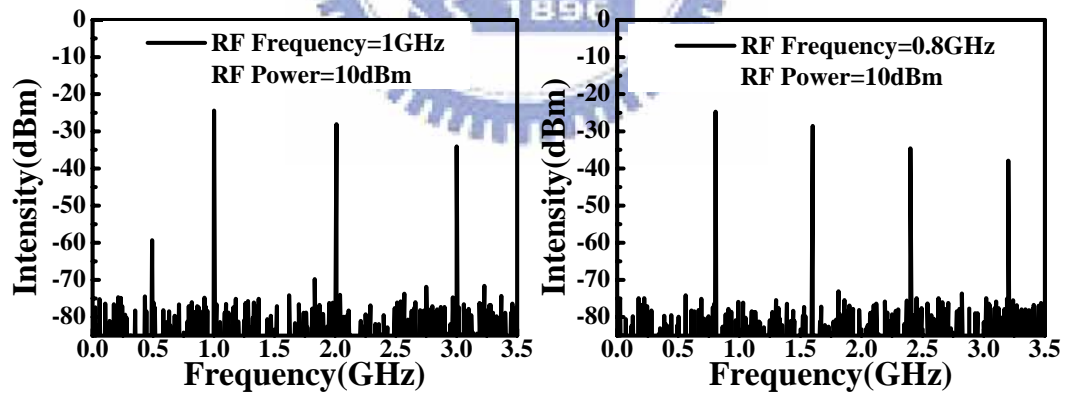


Fig 2-14 the nonlinear distortion at different modulation frequency ( BW : 30kHz )

## Chapter 3 Dynamical characteristics of 1.3 $\mu\text{m}$ QD VCSEL

### 3-1 Sample structure and Fabrication process

The structures were grown on GaAs (100) substrates by using molecular beam epitaxy (MBE) method. The  $n^+$  GaAs as buffer layer, The top distributed Bragg reflector (DBR ) is 33.5 pair  $n^+$   $\text{Al}_{0.9}\text{Ga}_{0.1}\text{As}/n^+$  GaAs (Si-doped), undoped active region, p-  $\text{Al}_{0.98}\text{Ga}_{0.02}\text{As}$  oxidation layer, The top bottom DBR is 22 pair  $p^+$   $\text{Al}_{0.9}\text{Ga}_{0.1}\text{As}/p^+$ -GaAs and  $p^+$ -GaAs (carbon-doped) is contact layer. The active region consisted of QDs structure to achieve some excellent characteristic. The thickness of the cavity active region is  $3\lambda$ . Carbon was used as the p-type dopant in the DBR to increase the carrier concentration ( $2\text{-}3\times 10^{18}\text{ cm}^{-3}$ ). In order to reduce the series resistance, the interfaces of both the p-type and n-type  $\text{Al}_{0.9}\text{Ga}_{0.1}\text{As}/\text{GaAs}$  DBR layers are linearly graded. The optical characteristics of QDs were optimized through PL measurement and structural analysis. The details of the process were fully described in our previous works [1]. The mesa diameter of the device is  $26\mu\text{m}$  with a  $5\mu\text{m}$  oxide aperture, and the device surface is quasi-planar so that the annular p-contact metal and the bond pad are on the same level. The device structure is shown in Fig.3-1. The p-contact was formed by directly depositing Ti/Pt/Au on the upper heavily doped  $p^+$  GaAs contact layer, and Au/Ge/Ni/Au was deposited on the bottom side of the substrate after it had been thinned down, and the shaded region beneath the

bond pad represents the implanted region.

## **3-2 DC Characteristics of QD VCSEL**

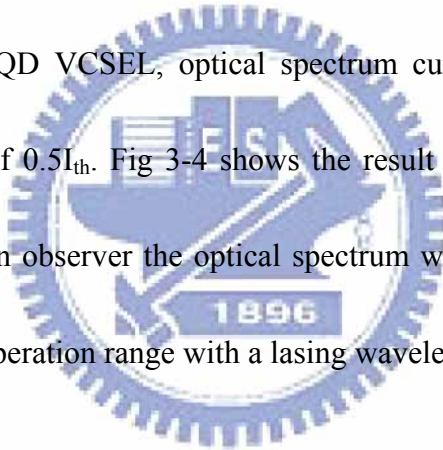
### **3-2-1 Experimental Setup**

We measure the DC characteristics of the 1.3  $\mu\text{m}$  QD VCSEL such as L-I curve, I-V curve and optical spectrum. We need to setup a system which can test our sample on wafer level or packaged device. Probe station was a basic instrument to meet our needs. Scheme of probe station system, illustrated in Figure 3-2, include probe station, current source, and powermeter module. Keithley 238 is the current source can provide precisely continuous current to laser diode and measure relative voltage synchronously. Newport power meter module (model 1835C) with photodiode and powermeter can be used to measure the light output power of the laser diode by using an integration sphere or measuring directly. The integration sphere is used to pick up part of whole emitting power from VCSEL to improve the accuracy of power measurement. The VCSEL device was placed on a platform of the probe station and was injected bias current with microprobe. From the L-I curve and I-V curve we can get some useful information such as the threshold current, slope efficiency, turn-on voltage and differential resistance. Near-field pattern was obtained by specific CCD. The optical spectrum of the device was measured by optical spectrum analyzer (OSA, Advantest Q8381). The emission light of the device is via optical fiber was package to

optical spectra analyzer. The OSA had spectrum resolution of 0.1nm which was adequate to measure VCSEL lasing spectra.

### **3-2-2 Results and Discussion**

Fig. 3-3 shows the output power of the device versus current curve (L-I) and the voltage of the device versus current curve (I-V). The threshold current is  $\sim 1.1$  mA. The output power rollover occurs as the current increases above 4.2mA with maximum optical output of 0.118mW at 20°C. To investigate the wavelength and current relation of the QD VCSEL, optical spectrum curves were measured from  $1.5I_{th}$  to  $3I_{th}$  with step of  $0.5I_{th}$ . Fig 3-4 shows the result of the optical spectrum at different current. We can observe the optical spectrum with single transverse mode operation in the whole operation range with a lasing wavelength about 1.278 $\mu$ m.



### **3-3 RIN measurement**

#### **3-3-1 Theory**

The RIN peak is a good indicate of the relaxation frequency of the device. The deriving force not input current is the Langevin force ( $F_s$ ,  $F_n$  and  $F_\varphi$ ) of the field due to the spontaneous emission. The Langevin force is assumed to be uncorrelated white Gaussian noise [3]. The relative intensity noise (RIN) spectrum is frequency dependence. The former can be derived from the rate equations.

The intrinsic relative intensity noise of a device is defined as

$$RIN = \frac{\langle \delta P(t)^2 \rangle}{P_0^2} \quad \text{Eq. 3-3.1}$$

$P_0$  is the average power and  $\delta P(t)^2$  is the mean square power fluctuation. From a small-signal analysis of the rate equations for a single-mode laser, we can derive the noise spectrum of the device. The relative intensity noise spectrum of external light injected locked device can be derived using the follow rate equations [2].

$$\begin{aligned} \frac{dS}{dt} &= \frac{G_0(N - N_{th})}{1 + \varepsilon S} \cdot S - \frac{S}{\tau_p} + 2k_c \sqrt{S \cdot S_{inj}} \cdot \cos(\phi(t) - \phi_{inj}) + R_{sp} + F_s \\ \frac{d\phi}{dt} &= \frac{\alpha}{2} \cdot G_0(N - N_{th}) - 2\pi \cdot \Delta f - k_c \sqrt{\frac{S_{inj}}{S}} \cdot \sin(\phi(t) - \phi_{inj}) + F_\phi \\ \frac{dN}{dt} &= \frac{I}{q} - \frac{N}{\tau_s} - \frac{G_0(N - N_{th})}{1 + \varepsilon S} \cdot S + F_n \end{aligned} \quad \text{Eq. 3-3.2}$$

$S$ ,  $\phi$  and  $N$  are the photon number, the phase and the carrier number inside the slave laser cavity.  $G_0$  is the gain coefficient,  $N_0$  is the transparency carrier number,  $\tau_p$  is the photon lifetime,  $\tau_n$  is the carrier lifetime,  $I$  is the slave laser bias current,  $\varepsilon$  is the gain compression factor, and  $\alpha$  is the linewidth enhancement factor.  $F_s$ ,  $F_\phi$  and  $F_n$  are the noise terms.  $\Delta\omega$  is the detuning between the master and slave laser.  $S_{inj}$  is the photons injection into the slave laser.  $k_c$  is the coupling coefficient, which determined by the photon injected into the cavity-round trip time. We use the injection-locked rate equation to simulation the experimental results.

We used the RIN measurement to find the device relaxation frequency with the

external light injection. The light injected into the cavity of the slave laser and depletes the carrier density. It makes the spontaneous emission rate reduced and more photons are coupled in phase into the amplified injection field. The more photons in phase and the relaxation frequency should enhance. The RIN spectrum represent the relaxation frequency peak becomes higher with injections. At a lower injection level directly adds photons into the slave laser cavity by using more carriers, which compensates the gain saturation and enhances the relaxation peaks of the slave laser. At stronger injections, the injected photons deplete the most of the available carriers, eventually saturate the signal and decrease the relaxation peaks. It prevents the further improvement of the relaxation frequency.

### 3-3-2 Experimental Setup

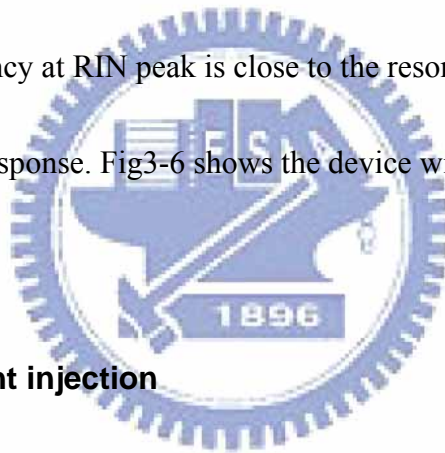
We measure the relative intensity noise characteristics of the 1.3  $\mu\text{m}$  QD VCSEL. We need to setup a system which can test our sample packaged device and can maintain the device temperature. The Scheme of the measurement system, illustrates in Figure 3-5, include current source, temperature controller, semiconductor optical amplifier (SOA), and RF spectrum analyzer. Keithley 238 is the current source can provide precisely continuous current to laser diode and measure relative voltage synchronously. The temperature controller model is TED200 with station can maintain the environmental temperature. The RIN spectrum is measured by the RF



spectrum analyzer (module Hp 8563E). The resolution of RF spectrum analyzer is 1MHz at experiment result. The external light source is tunable laser. The polarization of the tunable laser is adjusted using a polarization controller before injecting into the QD VCSEL.

### **3-3-3 Without light injection**

From the RIN spectrum without light inject, we can observe the RIN peak will shift to higher when the bias current higher. At 2.2Ith we can find the RIN peak move to 1.83GHz. The frequency at RIN peak is close to the resonant frequency can be found from frequency response. Fig3-6 shows the device without light injection experiment result.



### **3-3-4 With light injection**

Using the injection locking technique, we can enhance the bandwidth of the device. From the frequency response, we observe the bandwidth improve better when increasing the injection power and the bandwidth increase from 1.75GHz to 7.11GHz. The bandwidth will be limited by the package and external circuit. The RIN measurement is capacitance free. The RIN peak is a good indicate the relaxation frequency of the device. We experiment the external light injection at different current and different injection power. We observe the RIN peak can be reach to 19.2GHz at

bias 1.3mA, wavelength detune 0.081nm and external light power 3dBm. From the optical spectrum, we can observe when the light is injected into the QD VCSEL. The external photons in the cavity of the device will compete to deplete the gain and replace the original wavelength of the device. Fig3-7 shows the device with light injection RIN measurement result. Fig3-8 shows the device optical spectrum with and without light injection.

### 3-4 Simulations

#### 3-4-1 Theory

We based model of injection-locked rate equation (Eq 3-3.2) is usually used to describe the interaction between photons and carriers inside a laser cavity. When an additional light source is injected into the cavity, the system preserves the general form of the original equations, but with extra terms describing the effects of the injection.

$$F_s = F_s(\omega)e^{j\omega t}, F_\phi = F_\phi(\omega)e^{j\omega t}, F_N = F_N(\omega)e^{j\omega t}$$

$$S = S_0 + S_1(\omega)e^{j\omega t}, \phi = \phi_0 + \phi_1(\omega)e^{j\omega t}, N = N_0 + N_1(\omega)e^{j\omega t}$$

Substituting into the injection-locked rate equation

For the photon part:

$$i\omega S_1(\omega) = \frac{G_0(N_0 - N_{tr})}{1 + \varepsilon S_0} S_1(\omega) \left(1 - \frac{\varepsilon S_0}{1 + \varepsilon S_0}\right) + \frac{G_0 N_1(\omega)}{1 + \varepsilon S_0} S_0 - \frac{S_1(\omega) e^{j\omega t}}{\tau_p}$$

$$+ 2k_c \left( \sqrt{\frac{S_{inj}}{S_0}} \frac{S_1(\omega)}{2} \cos(\phi_0 - \phi_{inj}) - \sqrt{S_0 S_{inj}} \sin(\phi_0 - \phi_{inj}) \phi_1(\omega) \right) + F_s(\omega)$$

Eq. 3-4.1

For the phase part:

$$i\omega \phi_1(\omega) = \frac{\alpha G_0 N_1(\omega)}{2} - k_c \left( \sqrt{\frac{S_{inj}}{S_0}} \left( -\frac{S_1(\omega)}{2} \sin(\phi_0 - \phi_{inj}) + \cos(\phi_0 - \phi_{inj}) \phi_1(\omega) \right) + F_\phi(\omega) \right)$$

Eq. 3-4.2

Finally, for the carrier part:

$$i\omega N_1(\omega) = -\frac{N_1(\omega) e^{j\omega t}}{\tau_s} - \frac{G_0(N_0 - N_{tr})}{1 + \varepsilon S_0} S_1(\omega) \left(1 - \frac{\varepsilon S_0}{1 + \varepsilon S_0}\right) - \frac{G_0 N_1(\omega)}{1 + \varepsilon S_0} S_0 + F_n(\omega)$$

Eq. 3-4.3

Equations (2-4.1), (2-4.2), (2-4.3) are written in matrix form:

$$A \begin{bmatrix} S_1 \\ \phi_1 \\ N_1 \end{bmatrix} = \begin{bmatrix} F_s \\ F_\phi \\ F_n \end{bmatrix}$$

$$A = \begin{bmatrix} i\omega - \frac{G_0(N_0 - N_{tr})}{1 + \varepsilon S_0} \left(1 - \frac{\varepsilon S_0}{1 + \varepsilon S_0}\right) & 2k_c \sqrt{S_0 S_{inj}} \sin(\phi_0 - \phi_{inj}) & -\frac{G_0}{1 + \varepsilon S_0} S_0 \\ +\frac{1}{\tau_p} - k_c \sqrt{\frac{S_{inj}}{S_0}} \cos(\phi_0 - \phi_{inj}) & & \\ -\frac{k_c}{2} \sqrt{\frac{S_{inj}}{S_0^3}} \sin(\phi_0 - \phi_{inj}) & i\omega + k_c \sqrt{\frac{S_{inj}}{S_0}} \cos(\phi_0 - \phi_{inj}) & -\frac{\alpha}{2} G_0 \\ \frac{G_0(N_0 - N_{tr})}{1 + \varepsilon S_0} \left(1 - \frac{\varepsilon S_0}{1 + \varepsilon S_0}\right) & 0 & i\omega + \frac{G_0}{1 + \varepsilon S_0} S_0 + \frac{1}{\tau_s} \end{bmatrix}$$

The laser RIN

$$RIN(\omega) = |S_1(\omega)|$$

The small-signal modulation response can also be found from this system by considering  $I$  as the small signal modulation current.

$$\begin{bmatrix} S_1 \\ \phi_1 \\ N_1 \end{bmatrix} = A^{-1} \begin{bmatrix} 0 \\ 0 \\ I \end{bmatrix}$$

The modulation response transfer function will be

$$H(\omega) = \frac{|S_1(\omega)|}{I(\omega)}$$

### 3-4-2RIN simulation

From the injection locking rate equation, we can stimulate the RIN spectrum of the device at external light injection. The drive force is Langevin force white Gaussian noise with variance is zero. From the stimulation result, we find the higher external light strength and the higher frequency of RIN peaks. It is more photons in phase, when light strength increase. The more photons in the amplifier field increase the relaxation frequency. Fig3-9 shows the RIN spectrum stimulation result.

### 3-4-3Frequency Response simulation

From the rate equation, we can stimulate the frequency response at small signal operate. The drive force of frequency response different from the RIN spectrum is the

current variation. Fig3-10 shows the frequency response stimulation result. The inset chart is the resonant frequency versus the injection power.

### 3-4-4 Results and Discussion

Finally, we compare the RIN spectrum and the frequency response stimulation results at the same external light. We can observe the RIN peak is approach to the resonant frequency. The parameter, we stimulate need were listed Fig 3-11. Fig 3-12 shows the RIN spectrum and frequency response at the same chart. We can observe the RIN peaks and resonant frequency.

### 3-5 Linewidth enhancement factor

#### 3-5-1 Theory

In general, the width of a laser output is dependent of the fluctuations in the phase of the optical field. The fluctuations are due to the spontaneous emission alter the phase and intensity of the output field. Linewidth enhancement factor is ratio of the deviation of the imaginary part of the refractive index will change by the carrier density and the real part of the refractive index will change by the carrier density [4].

It can be defined as:

$$\alpha = -\frac{dn'/dn}{dn''/dn} \quad \text{Eq. 3-5.1}$$

The refractive:

$$n = n' - jn''$$

The value of the linewidth enhancement factor is dependent on the dimension of the quantization. The complex refractive index changes by the carrier density. We can observe from the following formulas [5].

$$n'(\omega) = \frac{1}{2\varepsilon_0 n} \sum \int \langle R_{ch}^2 \rangle \frac{g_{ch}(f_c - f_v)(E_{ch} - \hbar\omega)}{(E_{ch} - \hbar\omega)^2 + (\hbar/\tau_{in})^2} dE_{ch} \quad \text{Eq. 3-5.2}$$

$$n''(\omega) = \frac{\lambda}{4\pi} g$$

$$= \frac{1}{2\varepsilon_0 n} \sum \int \langle R_{ch}^2 \rangle \frac{g_{ch}(f_c - f_v)\hbar/\tau_{in}}{(E_{ch} - \hbar\omega)^2 + (\hbar/\tau_{in})^2} dE_{ch} \quad \text{Eq. 3-5.3}$$

The change of the linewidth enhancement factor with different quantization dimension alters the term of  $g_{ch}$ .  $g_{ch}$  is the density-of-states of the electron-hole pair. It is expressed by the step and delta functions, for a quantum well and quantum box. The change in the imaginary part of the susceptibility (gain or loss) will be influenced by a corresponding change in its real part (refractive index) through the Kramers-Kronig relations. A symmetrical gain curve will lead to a dispersion curve of the refractive index. It makes the linewidth enhancement factor zero at the frequency corresponding to the gain peak.

We use the locking region to calculate the value of the linewidth enhancement factor. The light of master laser injected into the slave laser at near the output

wavelength of the slave laser. The formula can be derived from the photon and the phase rate equation.

$$\begin{aligned}\frac{dP}{dt} &= [G - 1/\tau_p + \frac{c}{n_g L} (\frac{P_i}{P})^{1/2} \cdot \cos\theta] \cdot P \\ \frac{d\theta}{dt} &= [\omega_{mo} - \omega_o + \frac{c}{2n_g L} (\frac{P_i}{P})^{1/2} \cdot \sin\theta + \frac{\alpha}{2}(G - 1/\tau_p)]\end{aligned}\quad \text{Eq. 3-5.4}$$

P is the total photon number and  $\phi$  is the phase. G is the optical gain and N is the carrier density.  $\tau_p$  is the photon lifetime and  $n_g$  is the group index. The expression of the locking bandwidth is given as a function:

$$\Delta\omega = \frac{c}{2n_g L} (\frac{P_i}{P})^{1/2} \cdot (\sin\theta - \alpha \cdot \cos\theta) \quad \text{Eq. 3-5.5}$$

When injection locked stable, we can derive the locking bandwidth formula.

$$\begin{aligned}-\rho\sqrt{1 + \alpha^2} &< \Delta\omega < \rho \\ \rho &= \frac{c}{2n_g L} (\frac{P_i}{P})^{1/2}\end{aligned}\quad \text{Eq. 3-5.6}$$

At the same injection power, the ratio of the positive and negative detune. We can calculate the value of linewidth enhancement factor.

### 3-5-2 Experimental Setup

We measure the locking region of the 1.3 um QD VCSEL and QW VCSEL. We need to setup a system which can test our sample packaged device and can maintain the device temperature. The Scheme of the measurement system, illustrates in

Fig 3-13, include current source, temperature controller, polarization controller, variable attenuator, optical spectrum analyzer (OSA, Advantest 8381), semiconductor optical amplifier (SOA), and wavelength meter. Keithley 238 is the current source can provide precisely continuous current to laser diode and measure relative voltage synchronously. The temperature controller model is TED200 with station can maintain the environmental temperature. The optical spectrum analyzer is used to observe the master laser light inject into the slaver laser situation. The max resolution of the optical spectrum analyzer is 0.1nm, but we need more accurate resolution in our experiment. The resolution of wavelength meter can reach to 0.001nm. The external light source is tunable laser and can be accurate operated. The polarization of the tunable laser is adjusted using a polarization controller before injecting into the QD VCSEL. We also use a variable attenuator to controller the light power before inject into the polarization controller. We justify the lock or unlocked by the wavelength meter. We can observe the light from master laser complete with slave laser origin output light. Finally, the output light via the slave laser will become one wavelength observe by the wavelength meter. We use the method to find out the positive and the negative detune at the same external light injection.

### **3-5-3 1.3 $\mu$ m QD VCSEL**

We use the locking region measurement method to calculate the QD VCSEL



linewidth enhancement factor. We chose 4 points which are  $1.5 \sim 3I_{th}$ . The linewidth enhancement factor of the QD VCSEL is  $0.48 \sim 0.6$ . The value of the linewidth enhancement factor will increase with the current increasing.

#### **3-5-4 1.3 $\mu$ m QW VCSEL**

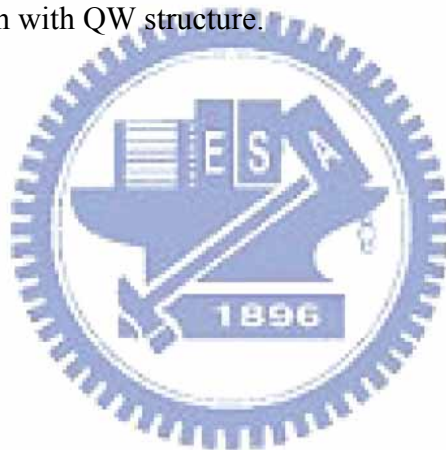
We use the locking region measurement method to calculate the QWVCSEL linewidth enhancement factor. We chose 4 points which are  $1.5 \sim 3I_{th}$ . The linewidth enhancement factor of the QD VCSEL is  $4.34 \sim 4.84$ . The value of the linewidth enhancement factor will increase with the current increasing. Compare with the VCSEL with QD and QW structure, we can observe the value of linewidth enhancement factor with QD structure is much lower than with QW structure.

Figure 3-14 shows the linewidth enhancement factor

#### **3-6 Summary**

We present monolithic quantum-dot vertical-cavity surface-emitting laser (QD VCSELs) operating in the  $1.3 \mu\text{m}$  optical communication wavelength. The QD VCSELs have adapted fully doped structure on GaAs substrate. The output power is  $\sim 120 \mu\text{W}$  with slope efficiency of  $0.044 \text{ W/A}$  at room temperature. We also measure the optical spectrum of QD VCSEL and QW VCSEL at different current. We observe the device with QD structure wavelength shift is smaller than with QW

structure. Using the external light injection technique, we observe from the RIN spectrum the relaxation frequency reach to 19.2GHz of the QD VCSEL. We also stimulate the experiment result of RIN measurement and the frequency response at the same situation. From the stimulate result, we find the RIN peaks is approach to the resonant frequency. Finally, using the locking region method we can obtain the value of linewidth enhancement factor. Compare the value of the device with QD structure and with QW structure, we observe device with QD structure linewidth enhancement factor is much lower than with QW structure.



## Reference

- [1] H. C. Yu, S. J. Chang, Y. K. Su, C. P. Sung, Y. W. Lin, H. P. Yang, C. Y. Huang and J. M. Wang, "A simple method for fabrication of high speed vertical cavity surface emitting lasers," *Materials Science Engineering B*, vol. 106, pp. 101-104, 2004.
- [2] Lukas Chrostowski, "Optical Injection Locking of Vertical Cavity Surface Emitting Lasers," Fall 2003
- [3] X. Jin and S. L. Chuang , "Relative intensity noise characteristics of injection-locked semiconductor lasers, " *APPLIED PHYSICS LETTERS*, vol 77, NUMBER 9 , 28 AUGUST 2000
- [4] Marek Osinski and Jens Buus, "Linewidth Broadening Factor in Semiconductor Laser-An Overview, " *IEEE journal of quantum electronics*, vol. QE-23, 1987
- [5] Yasunari Miyake and Masahiro Asada, "Spectral Characteristics of Linewidth Enhancement Factor  $\alpha$  of Multidimensional Quantum Wells, " *Japanese journal of applied physics*, vol 28 pp1280-1281, 1989

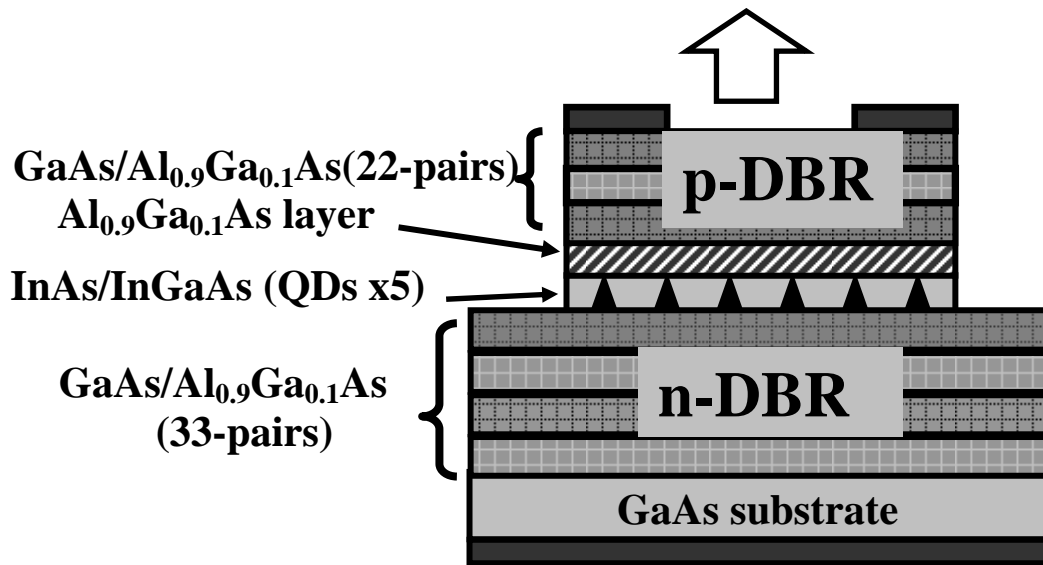


Fig 3-1 The structure of 1.3 $\mu$ m QD VCSEL

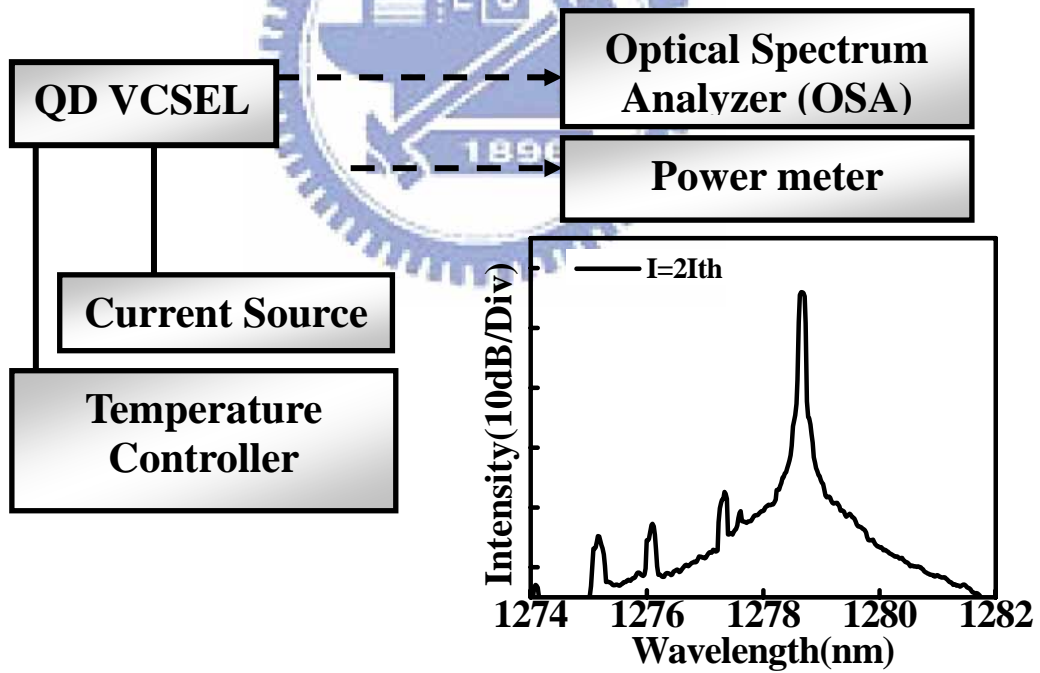


Fig 3-2 experimental setup for measurement DC characteristic

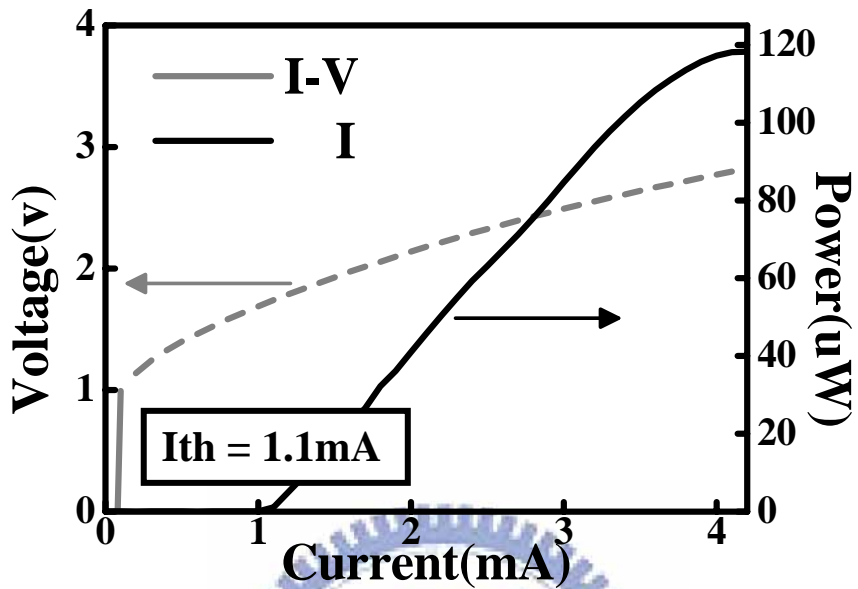


Fig 3-3 I-V and L-I curve of the 1.3µm QD VCSEL (No. 15)

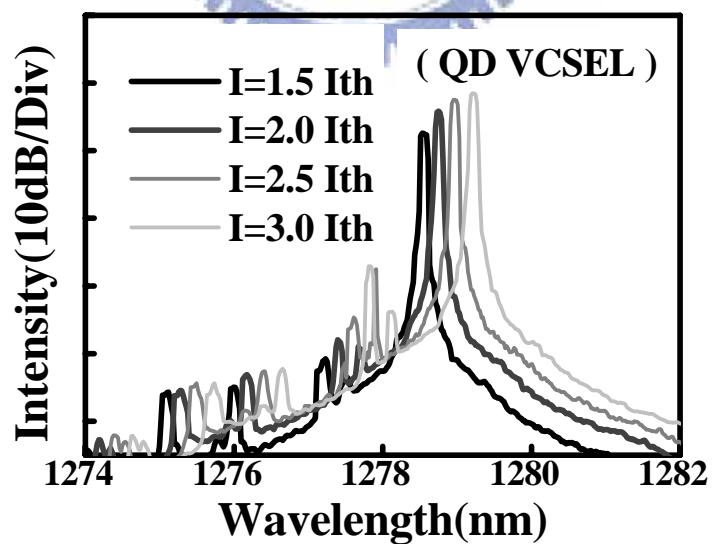


Fig 3-4 Optical spectrum of the device at different current

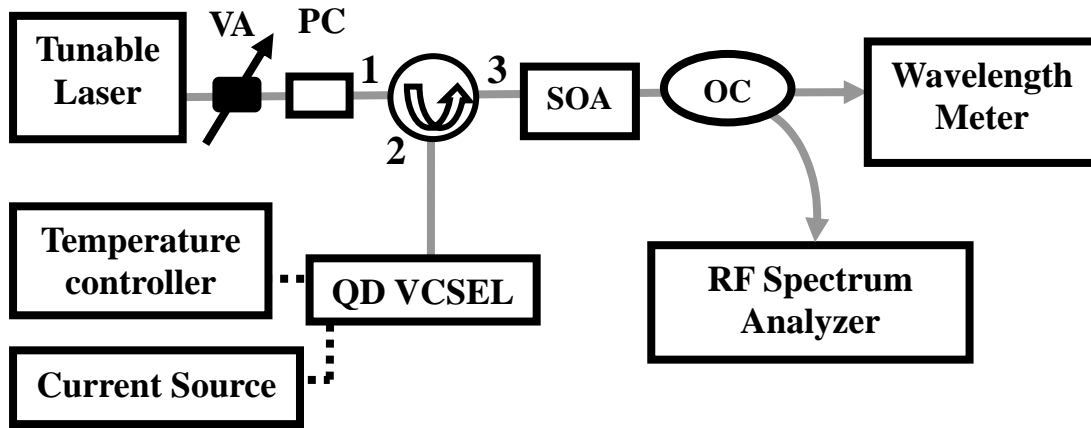


Fig 3-5 experiment setup for the RIN measurement

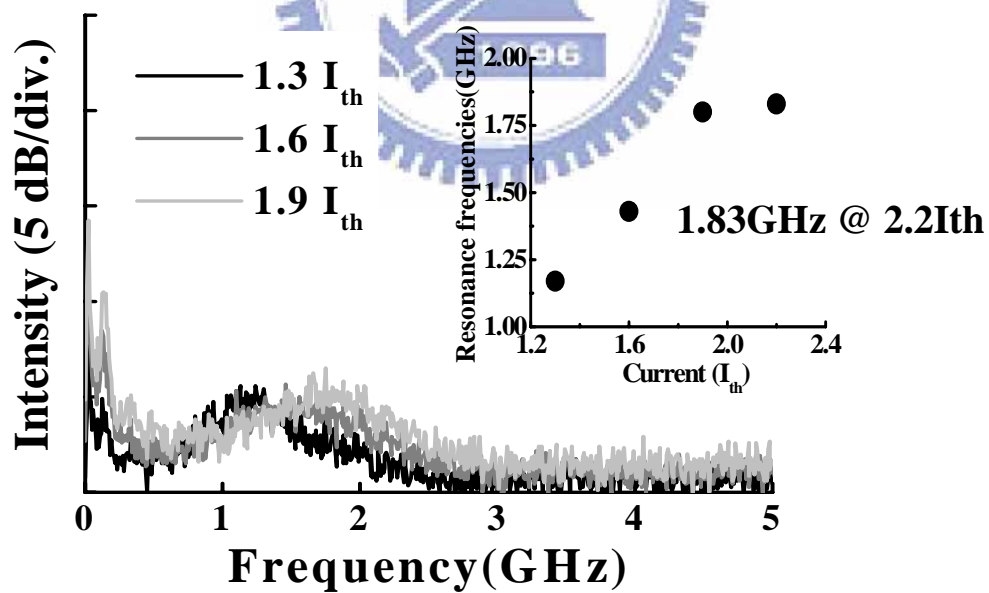


Fig 3-6 RIN spectrum of the device without external light injection

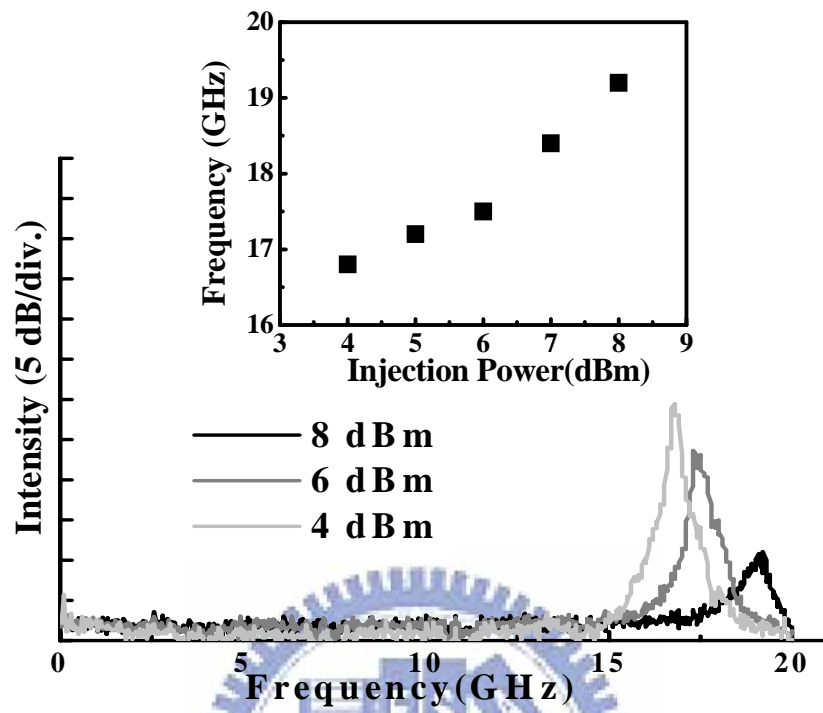


Fig 3-7 RIN spectrum for the device with external light injection

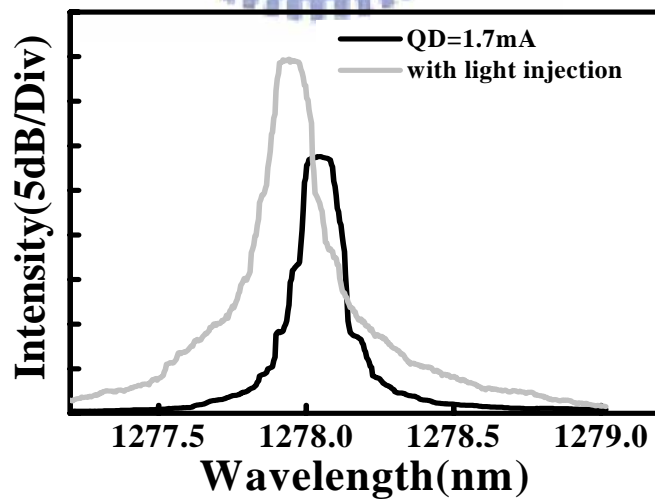


Fig 3-8 the optical spectrum of the device with and without light injection

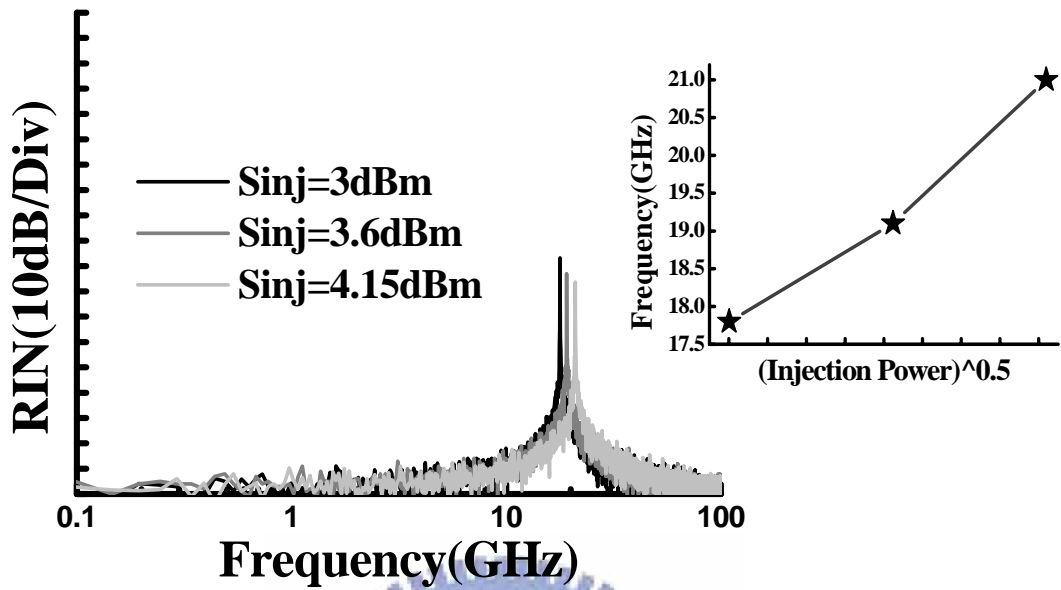


Fig 3-9 stimulation result of the RIN spectrum with external light injection

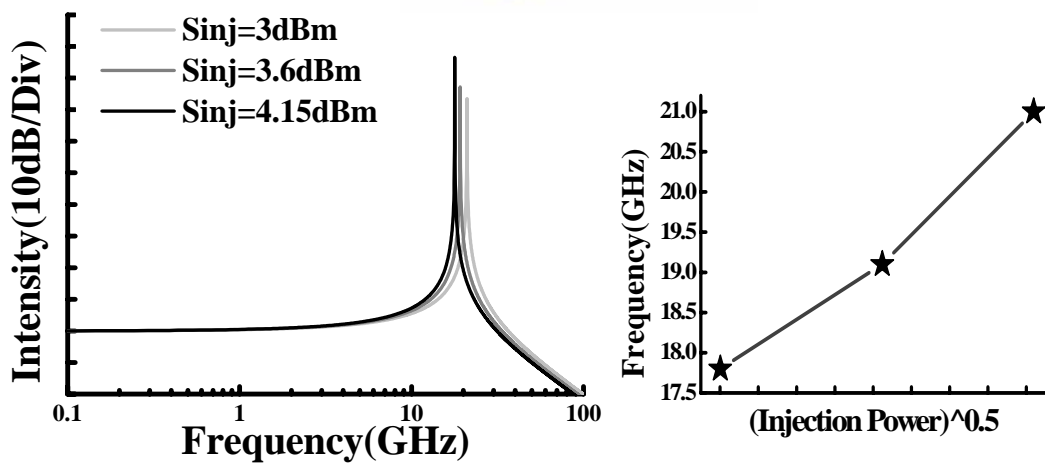


Fig 3-10 stimulation result of the frequency response with external light injection



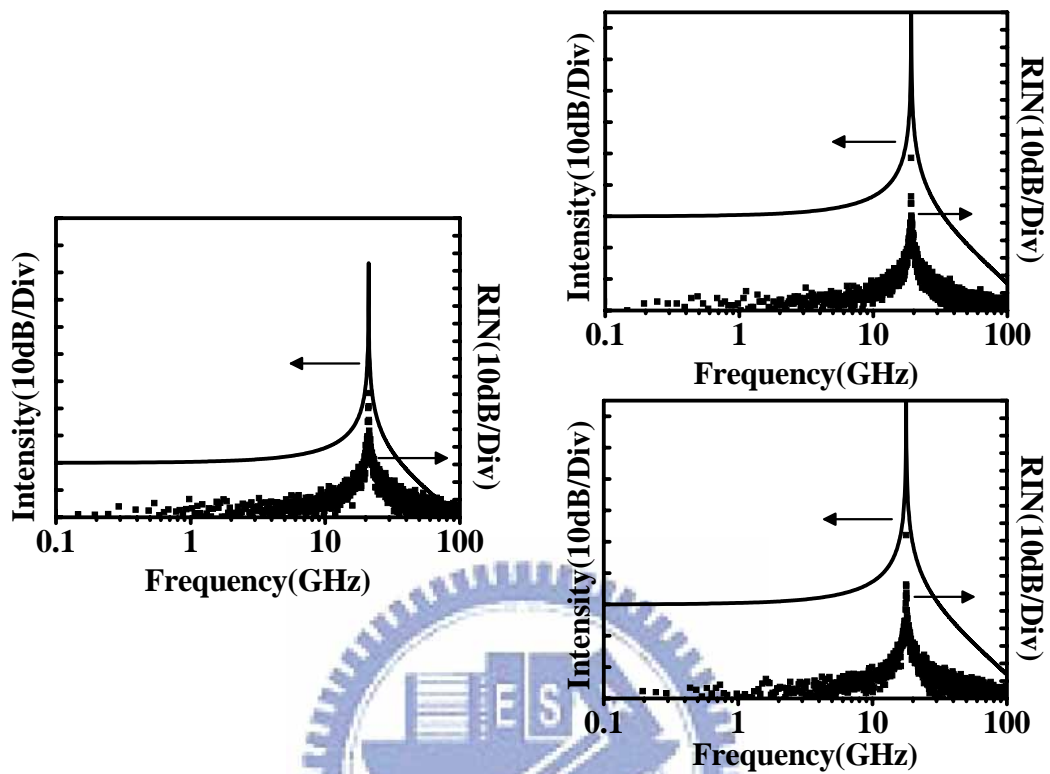


Fig 3-11 Compare the RIN peaks with the resonant frequency with external light injection

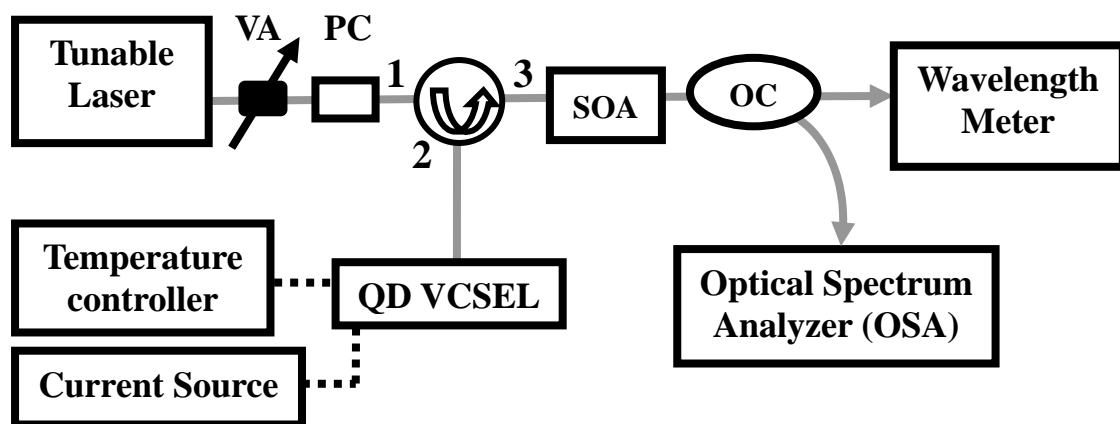


Fig 3-12 experiment setup for the locking region measurement

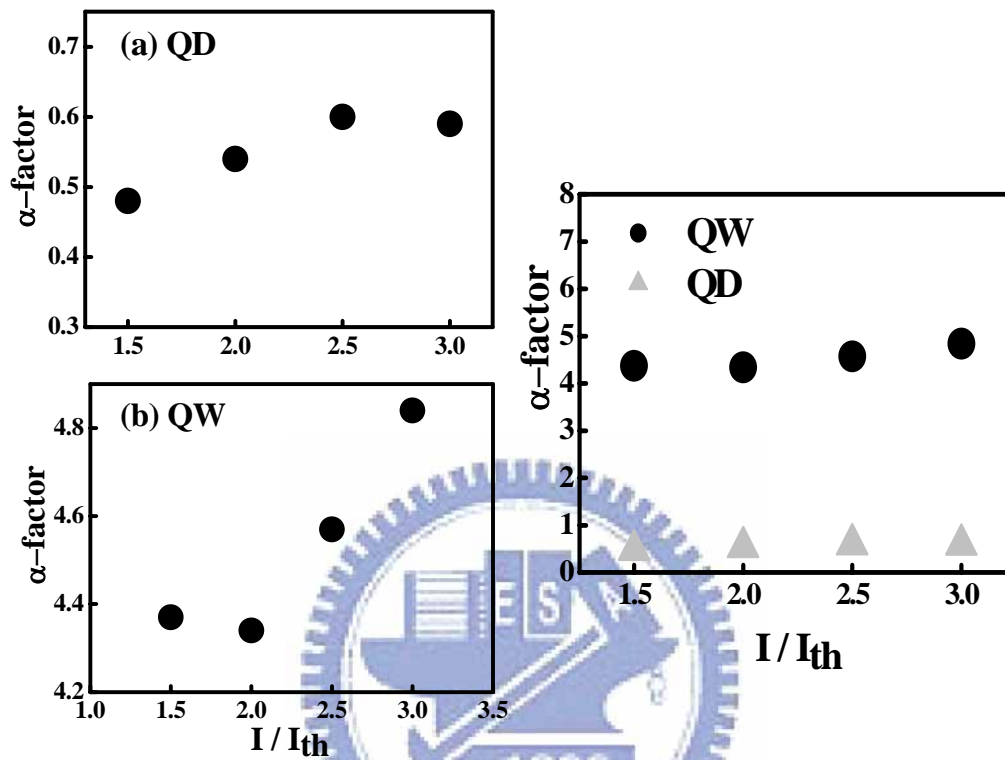


Fig 3-13 linewidth enhancement factor of the device with QD and QW structure at different current

## Chapter 4 Summary

### 4-1 Summary

In summary, we have studied high speed characteristics of quantum dot vertical-cavity surface-emitting laser. In Chapter 2, we demonstrate monolithically single-mode 1.3 $\mu\text{m}$  QD VCSELs on GaAs substrate with high side-mode suppression ratio. The output power is  $\sim 118 \mu\text{W}$  with slope efficiency of 0.044 W/A at room temperature. Single mode operation was obtained with side-mode suppression ratio of  $> 30 \text{ dB}$ . Using the external light injection technique, we observe from the RIN spectrum the relaxation frequency reach to 19.2GHz of the QD VCSEL. We also stimulate the experiment result of RIN measurement and the frequency response at the same situation. From the locking region method, we can obtain the value of linewidth enhancement factor. The value of the device with QD structure is 0.48~0.6 and with QW structure is 4.34~4.84. We observe device with QD structure linewidth enhancement factor is much lower than with QW structure.

In Chapter 3, we report the experimental high speed characterization of 0.98 $\mu\text{m}$  QD VCSEL. We also present the device structure about 0.98 $\mu\text{m}$  QD VCSEL, the L-I&I-V curves, the RIN measurement at different temperature, frequency response calibration method, the eye diagram at different temperature and the nonlinear distortion. We observe notch occurred due to multi-mode in small signal modulation. We also use the calibration method to find the device frequency response. A 2.5 Gb/s

non-return-to-zero (NRZ) pseudo-random binary sequence (PRBS) data with  $2^{31}-1$  pattern length from a pattern generator used to directly modulate the QD VCSEL. The eye diagrams can be clearly observed. We also measure the nonlinear distortion and find the SFDR is 76dB.

#### **4-2 Future Work**

Future work will be focus on the slow light in QD VCSEL. We will try to using the slow light technique to transmission data. Further discussions on quantum dot medium and cavity resonance effect will be studied.

